BRL

12

AD

MEMORANDUM REPORT NO. 2784

BLAST DIFFRACTION LOADING ON THE FRONT AND REAR SURFACES OF A RECTANGULAR PARALLELEPIPED

Noel H. Ethridge

September 1977

Approved for public release; distribution unlimited.

USA ARMAMENT RESEARCH AND DEVELOPMENT COMMAND
USA BALLISTIC RESEARCH LABORATORY
ABERDEEN PROVING GROUND, MARYLAND

Destroy this report when it is no longer needed.
Do not return it to the originator.

Secondary distribution of this report by originating or sponsoring activity is prohibited.

Additional copies of this report may be obtained from the National Technical Information Service, U.S. Department of Commerce, Springfield, Virginia 22151.

The findings in this report are not to be construed as an official Department of the Army position, unless so designated by other authorized documents.

The use of trade names or manufacturers' names in this report does not constitute indorsement of any commercial product.

Unclassified

SECURITY CLASSIFICATION OF THIS PAGE (When Data Entered)

REPORT DOCUMENTATION PAGE

READ INSTRUCTIONS BEFORE COMPLETING FORM

1. REPORT NUMBER: BRL MEMORANDUM REPORT NO. 2784 (14 BRL-MR-2784) — 2. GOVT ACCESSION NO. — 3. RECIPIENT'S CATALOG NUMBER

4. TITLE (and Subtitle): (6) BLAST DIFFRACTION LOADING ON THE FRONT AND REAR SURFACES OF A RECTANGULAR PARALLELEPIPED. — 5. TYPE OF REPORT & PERIOD COVERED: (9) Final rept., — 6. PERFORMING ORG. REPORT NUMBER

7. AUTHOR(s): (10) Noel H. Ethridge — 8. CONTRACT OR GRANT NUMBER(s)

9. PERFORMING ORGANIZATION NAME AND ADDRESS: USA Ballistic Research Laboratory, Aberdeen Proving Ground, Maryland 21005 — 10. PROGRAM ELEMENT, PROJECT, TASK AREA & WORK UNIT NUMBERS: (16) 1L162118AH75

11. CONTROLLING OFFICE NAME AND ADDRESS: US Army Materiel Development and Readiness Command, 5001 Eisenhower Avenue, Alexandria, Virginia 22333 — 12. REPORT DATE: (11) SEP[redacted]77 — 13. NUMBER OF PAGES: 85 (12) 71p.

14. MONITORING AGENCY NAME & ADDRESS (if different from Controlling Office) — 15. SECURITY CLASS. (of this report): UNCLASSIFIED — 15a. DECLASSIFICATION/DOWNGRADING SCHEDULE

DDC RECEIVED FEB 23 1978 B

16. DISTRIBUTION STATEMENT (of this Report)

Approved for public release; distribution unlimited.

17. DISTRIBUTION STATEMENT (of the abstract entered in Block 20, if different from Report)

18. SUPPLEMENTARY NOTES

19. KEY WORDS (Continue on reverse side if necessary and identify by block number)

Blast loading
Diffraction loading
Parallelepiped
Shock tube
Three-dimensional hydrocode
BAAL
Empirical Equations
Rigid-body overturning code

20. ABSTRACT (Continue on reverse side if necessary and identify by block number) (ljc)

Equations have been fitted to shock tube data to provide a prediction technique for the average pressure loading on the front and rear surfaces of rectangular parallelepipeds. Equations are presented as fitted to the data and also as modified for use in a rigid-body response code. The data fitted were obtained from models exposed in a shock tube and instrumented with pressure gages. Incident shock overpressures ranged from 34.5 to 138 kPa (5 to 20 psi), and both two and three-dimensional configurations were utilized. Comparisons with other

→ over

DD FORM 1 JAN 73 1473 EDITION OF 1 NOV 65 IS OBSOLETE

050750 1

Unclassified

SECURITY CLASSIFICATION OF THIS PAGE (When Data Entered)

20. ABSTRACT (Continued)

shock tube data and with the results of a three-dimensional hydrocode (BAAL) calculation are presented.

TABLE OF CONTENTS

LIST OF ILLUSTRATIONS

LIST OF ILLUSTRATIONS (Continued)

LIST OF ILLUSTRATIONS (Continued)

LIST OF ILLUSTRATIONS (Continued)

LIST OF ILLUSTRATIONS (Continued)

I. INTRODUCTION

The whole-body motion of an item of military equipment struck by a long-duration blast wave may result in functional or physical damage to that item. In order to develop techniques for predicting such motion, it is necessary to describe the loading on the target produced by the blast wave. In a computer code developed at the Ballistic Research Laboratory to calculate rigid body rotation, the target was modeled as a collection of rectangular parallelepipeds[1]. For such a code, a load prediction technique is required which considers the variations in dimensions of such parallelepipeds which occur in a given model.

The blast loading of a target occurs in two phases: the diffraction phase, where the shock wave encounters and engulfs the target; and the drag phase, which occurs when variations due to the diffraction process have ceased and quasi-steady drag loading is experienced by the target. This report is concerned with developing a prediction technique for the average pressures developed on the front and rear surfaces of a rectangular parallelepiped during the diffraction phase. The target is assumed to be struck by a shock front which is moving normal to the front surface.

No satisfactory diffraction loading prediction technique was available for predicting the average loading on all surfaces of a target. In Reference 2, Taylor describes a comparison between results obtained in shock tube experiments and loading predicted by techniques contained in standard manuals[3]. Significant differences were shown, and therefore such techniques require improvement.

The basic data used by Taylor for the analysis described in Reference 2 were available at BRL[4]. The purpose of this report is to present equations fitted to these data to provide a prediction technique for the average loading on the front and rear surfaces of rectangular parallelepipeds. Equations are presented as fitted to the data and also as modified for use in a rigid-body response code.

---

[1] *N. H. Ethridge, "Blast Overturning Model for Ground Targets," BRL Report 1869, June 1976.* (AD #B012102L)

[2] *W. J. Taylor, "A Method for Predicting Blast Loads During the Diffraction Phase," USA Ballistic Research Laboratories, Aberdeen Proving Ground, Maryland; included in Part 4, Bulletin 42, The Shock and Vibration Bulletin, The Shock and Vibration Information Center, Naval Research Laboratory, Washington, D. C., January 1972.*

[3] *C. M. Norris, et al., "Structural Design for Dynamic Loads," McGraw-Hill Book Company, Inc., New York, N. Y., 1959.*

[4] *W. J. Taylor, Private Communication.*

Figure 1 shows the target used by Taylor in the shock tube experiments. Pressure gages were positioned at locations labeled A, C, and D. Position B was not instrumented, since by symmetry the pressure at Position B should be the same as that at Position A. To obtain the average pressure the output of all three gages were electronically summed. The output from the gage at A was given twice the weight of the output of gages D and C to effectively include the record that would have been obtained by a gage at B.

Figure 2 shows the test configurations used by Taylor. By the addition of blocks on the ends of the model a two-dimensional configuration was produced. Data were obtained for both configurations and for front and rear surfaces for nominal shock overpressures of 34.5, 69, 103, and 138 kPa (5, 10, 15, and 20 psi). Tables 1 and 2 list the test shots and data appropriate for each[4].

Gentry[5] made a hydrocode calculation for this target for a shock wave of 34.47 kPa (5 psi) incident overpressure for the three-dimensional configuration shown in Figures 2(A) and 2(C). The hydrocode predictions for individual gage records matched the experimental data very well. Average pressures computed for the front and rear surfaces were in good agreement with average pressures calculated using computed values at the gage positions and the same averaging procedure as was used for the gage records in Reference 2. Thus the procedure used by Taylor to record average pressure on front and rear surfaces seems satisfactory for the three-dimensional configuration. No hydrocode calculation was available to check the averaging procedure for the two-dimensional configuration shown in Figures 2(B) and 2(D). The positions of the gages and the averaging procedure do not seem as appropriate for the two-dimensional configuration as for the three-dimensional configuration.

II. FRONT SURFACE LOADING

A. Fitting an Equation for Average Front Surface Pressure

In Reference 2, Taylor found that two and three-dimensional average pressure curves on the front surface of the shock tube target would nearly coincide if the time scale were described in units of the number of rarefaction wave crossings of the loaded area. A rarefaction wave originates at each free edge, so that for the three-dimensional configuration two rarefaction wave crossings occur in the time that one occurs for the two-dimensional configuration. Figures 3 and 4 show figures from Reference 2 which present the average front-surface pressure loading versus the number of rarefaction wave crossings. These data were used for fitting an equation. As noted above, the three-dimensional data

---

[5] *R. A. Gentry, et al., "Three Dimensional Computer Analysis of Shock Loads on a Simple Structure," BRL CR 219, USA Ballistic Research Laboratories, Aberdeen Proving Ground, MD, March 1975.* (AD #B003208L)

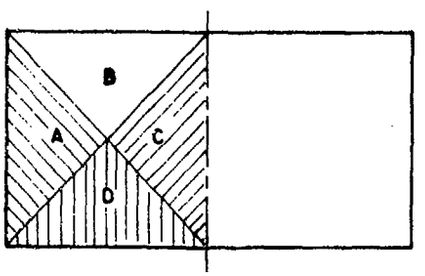

(A) SURFACE ZONING

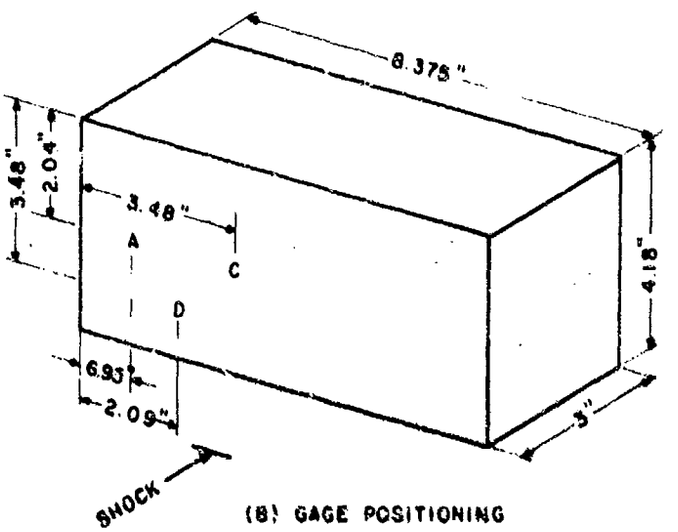

(B) GAGE POSITIONING

Figure 1 Target dimensions and gage positioning used in the study described in Reference 2.

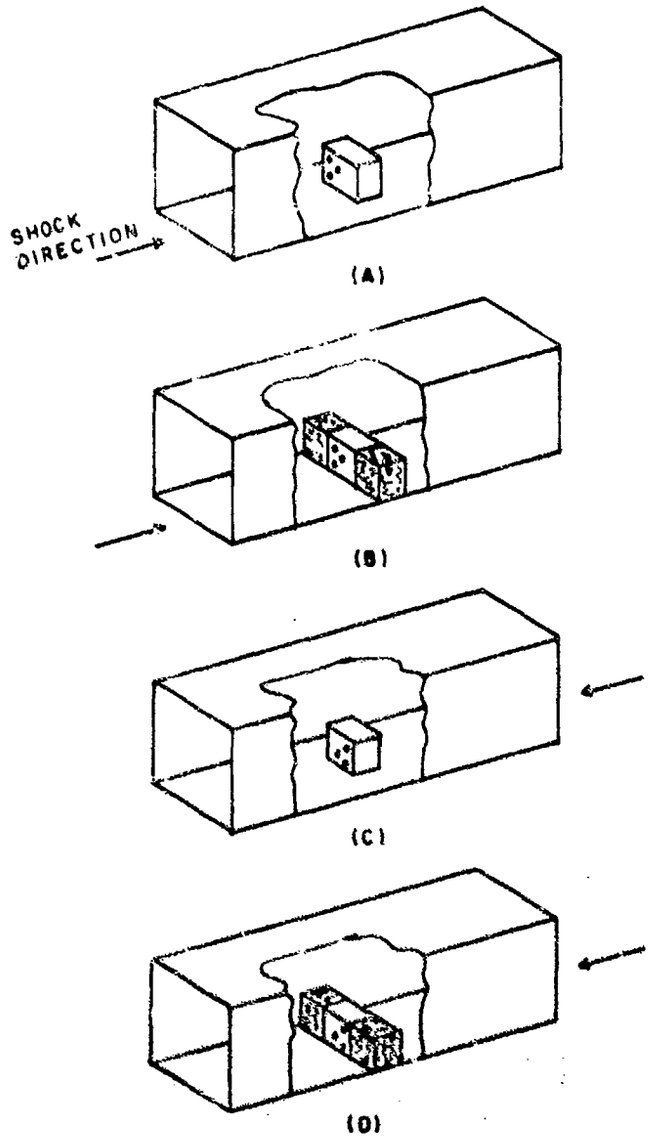

Figure 2 Test configurations for the shock tube experiments for the study reported in Reference 2.

Table 1. Shock Tube Test Shots from the Study by Taylor[2,4], SI Units

Shot	CONF	P_s (kPa)	P_A (kPa)	T_A (°K)	a_o (m/s)	a_S (m/s)	z	P_R (kPa)	P_{stag} (kPa)	P_{stag}/P_R	P_s/P_R	P_q (kPa)	P_{MR}/P_s
1	3DF	34.47	101.7	293.73	343.5	373.1	.3390	78.50	38.50	.4904	.4391	3.981	-
2	3DR	32.96	101.7	294.68	344.1	372.5	.3241	74.66	36.64	.4907	.4414	3.646	1.01
3	2DR	32.82	101.6	295.44	344.4	372.8	.3229	74.32	36.47	.4908	.4416	3.618	.88
4	2DR	62.47	101.6	295.55	344.6	394.7	.6147	155.19	75.42	.4860	.4025	12.606	.68
5	2DR	101.35	102.0	294.47	344.0	418.5	.9939	278.31	134.64	.4838	.3642	31.504	.475
6	2DR	139.4	102.0	294.70	344.1	440.7	1.3671	415.50	201.32	.4845	.3355	56.948	.38
7	3DR	74.60	102.0	294.95	344.3	402.0	.7316	191.56	92.89	.4849	.3894	17.647	.80
8	3DR	113.1	102.0	295.47	344.6	426.1	1.1089	318.92	154.28	.4837	.3546	38.656	.7?
10	3DR	148.5	102.0	295.55	344.6	446.5	1.4554	450.41	218.46	.4850	.3297	63.908	.63
11	3DF	73.70	102.6	294.12	343.8	400.8	.7184	188.57	91.46	.4850	.3909	17.151	-
12	3DF	111.1	102.6	294.20	343.8	424.0	1.0833	311.66	150.76	.4837	.3566	37.239	-
13	3DF	147.1	102.6	294.30	343.9	444.4	1.4341	444.38	215.48	.4849	.3311	62.546	-
14	2DF	144.2	102.8	294.56	344.1	442.6	1.4024	432.71	209.74	.4847	.3332	60.157	-
15	2DF	108.9	102.8	294.62	344.1	422.8	1.0590	303.58	146.84	.4837	.3586	35.765	-
16	2DF	72.19	102.8	294.67	344.1	399.9	.7022	183.86	89.20	.4852	.3926	16.454	-
17	2DF	36.13	102.8	294.82	344.2	374.6	.3514	82.62	40.49	.4901	.4373	4.318	-

Table 2. Shock Tube Test Shots from the Study by Taylor[2,4], English Units

Shot	CONF	P_s (psi)	P_A (psi)	T_A (°C)	a_o (ft/s)	a_s (ft/s)	z	P_R (psi)	P_{stag} (psi)	P_{stag}/P_R	P_s/P_R	P_q (psi)	P_{MR}/P_s
1	3DF	5	14.75	20.58	1127	1224	.3390	11.386	5.5834	.4904	.4391	.5774	-
2	3DR	4.78	14.75	21.53	1129	1222	.3241	10.829	5.3139	.4907	.4414	.5288	1.01
3	2DR	4.76	14.74	22.29	1130	1223	.3229	10.779	5.2898	.4908	.4416	.5248	.88
4	2DR	9.06	14.74	22.40	1130.7	1295	.6147	22.508	10.9390	.4960	.4025	1.8283	.68
5	2DR	14.70	14.79	21.32	1128.6	1373	.9959	40.366	19.5277	.4838	.3642	4.5693	.475
6	2DR	20.22	14.79	21.55	1129.1	1446	1.3671	60.263	29.1991	.4845	.3355	8.2596	.38
7	3DR	10.82	14.79	21.80	1129.5	1319	.7316	27.783	13.4722	.4849	.3894	2.5595	.80
8	3DR	16.40	14.79	22.32	1130.5	1398	1.1089	46.256	22.3758	.4837	.3546	5.6066	.70
10	3DR	21.54	14.80	22.40	1130.7	1465	1.4554	65.326	31.6845	.4850	.3297	9.2691	.63
11	3DF	10.69	14.88	20.97	1128	1315	.7184	27.350	13.2651	.4850	.3909	2.4875	-
12	3DF	16.12	14.88	21.05	1128.4	1391	1.0833	45.202	21.8655	.4837	.3566	5.4010	-
13	3DF	21.34	14.88	21.15	1128.3	1458	1.4341	64.452	31.2524	.4849	.3311	9.0716	-
14	2DF	20.91	14.91	21.41	1128.8	1452	1.4024	62.760	30.4207	.4847	.3332	8.7250	-
15	2DF	15.79	14.91	21.47	1128.9	1387	1.0590	44.030	21.2980	.4837	.3586	5.1873	-
16	2DF	10.47	14.91	21.52	1129	1312	.7022	26.667	12.9376	.4852	.3926	2.3864	-
17	2DF	5.24	14.91	21.67	1129.3	1229	.3514	11.983	5.8732	.4901	.4373	.6263	-

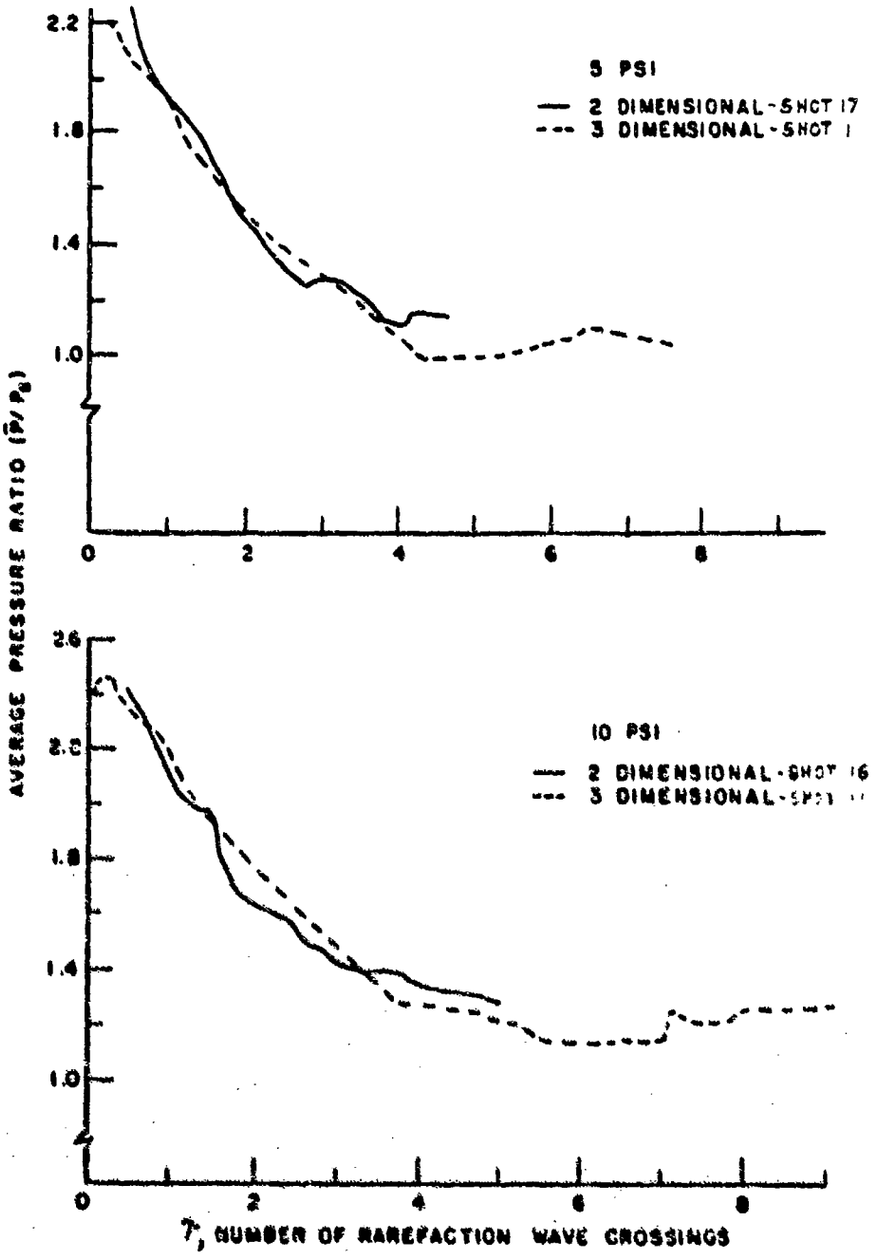

Figure 3 Average pressure as a function of rarefaction wave action for 5 and 10 psi shock waves. (from Reference 2)

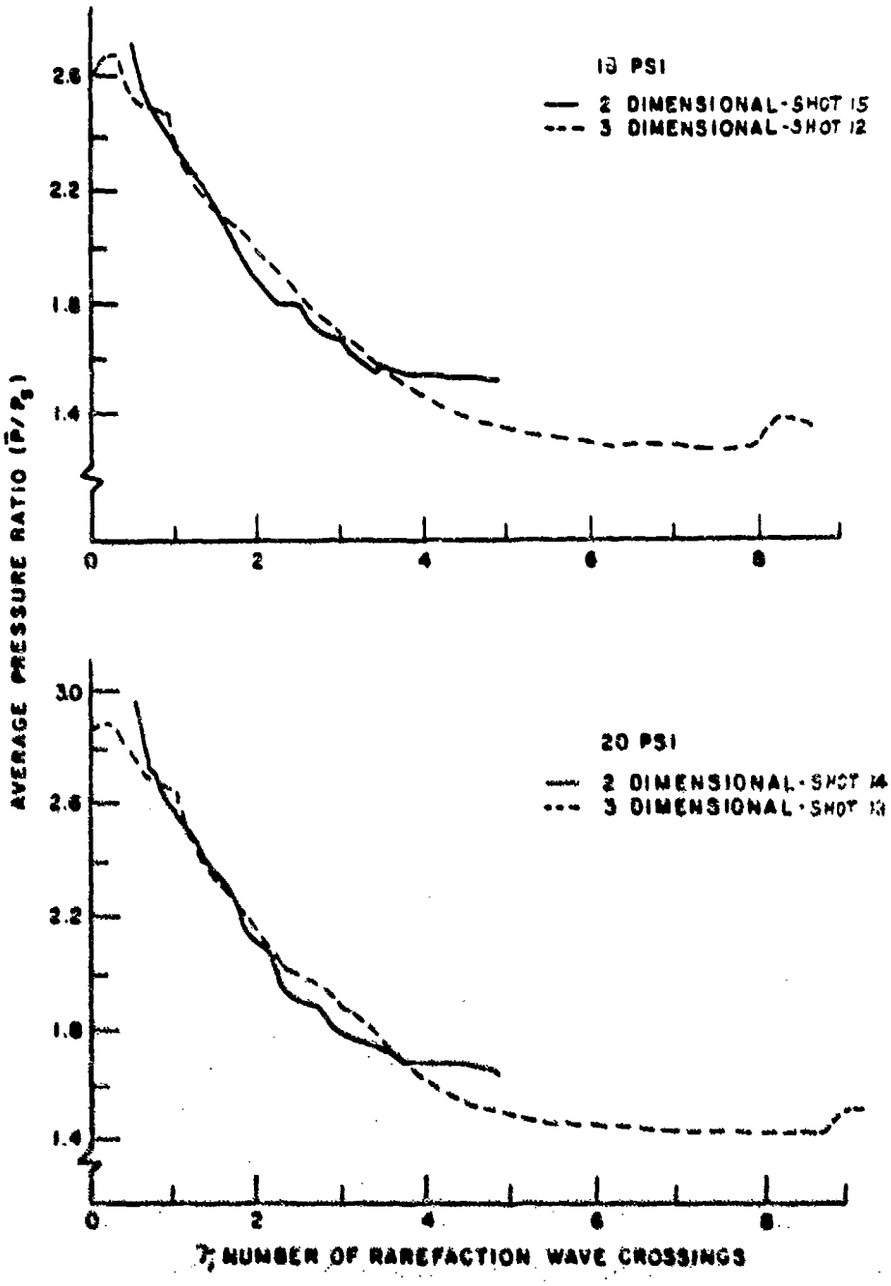

Figure 4 Average pressure as a function of rarefaction wave action for 15 and 20 psi shock waves. (from Reference 2)

apparently represent the average pressure very well, while the two-dimensional data may not present an accurate average. However, in the absence of other data the two dimensional curves were fitted and used in forming a prediction equation.

The basic form of the equation chosen for the fitting was as follows:

$$\frac{P}{P_R} = \left(1 - \frac{P_L}{P_R}\right) e^{-A\tau^B} + \frac{P_L}{P_R} \qquad (1)$$

where:

P = average overpressure

P_R = peak reflected overpressure

P_L = overpressure approached as a limit

τ = $t\, a_s(1 + R)/S$

t = time

a_s = velocity of the rarefaction wave behind the reflected shock wave

R = ratio of the edges of the minimum rectangular area which must be examined to define the loading over the entire surface area. The ratio is taken so that R ranges from 0 for the two-dimensional configuration to 1 for the three-dimensional configuration.

S = minimum distance of travel from an edge for a rarefaction wave to traverse the loaded area.

A, B = functions of time, incident overpressure, ambient pressure, and R.

This equation provides the appropriate zero initial slope and can be made asymptotic to the stagnation overpressure or some other selected pressure limit.

The limiting average overpressure for P_L was chosen to be the stagnation overpressure, P_{stag}. Actually the average limiting overpressure on the front surface should be somewhat less than P_{stag}, because some flow occurs across the surface as the air flows around the target. In Reference 3, the average overpressure limit is given as $P_s + 0.85\, P_q$, where P_s is the incident peak overpressure and P_q is the corresponding dynamic pressure. One would expect the amount of the reduction from stagnation overpressure to be a function of the shape parameter R, P_s, and P_A.

The limited set of data available from Reference 2 suggest that the three-dimensional data may indeed approach a limit less than that approached by the two-dimensional data. However, because of the limited data, P_{stag} was chosen as the average overpressure approached as a limit for this fitting exercise.

The function A was found by examining values read from the curves for $\tau = 1$. For that value the equation becomes:

$$\frac{P}{P_R} = \left(1 - \frac{P_L}{P_R}\right) e^{-A} + \frac{P_L}{P_R}$$

Solving this equation for A, the result is:

$$A = -\ln \left\{ \frac{\left(\frac{P}{P_R} - \frac{P_L}{P_R}\right)}{\left(1 - \frac{P_L}{P_R}\right)} \right\} \qquad (2)$$

Data for the two and three-dimensional configurations at $\tau = 1$ were found to be almost equal for the same incident shock overpressure, so these data were combined and fitted as a function of z, where z is the ratio of incident shock overpressure P_S to the ambient atmospheric pressure P_A.

The function found for A was inserted into Equation 1 and corresponding values of the function B were calculated to provide a smooth representation of the curves in Figures 3 and 4. A function was fitted to those values of B versus τ. A constant value provided a satisfactory representation of the three-dimensional data. However, for the two-dimensional data a variation with both z and τ was found necessary for a reasonable representation and th. form selected was:

$$B(z, \tau) = a + e^{-\alpha z^{\beta} \tau} \qquad (3)$$

where a, α and β were the chosen parameters.

Figure 5 shows the area on the front surface of a block target for which pressure loading must be determined in order to define the loading over the entire front surface area. If the target is in free air there are two planes of symmetry, and only one-fourth the area need be examined. For a target on the surface, which represents the configurations shown in Figures 2A and 2C, a vertical plane of symmetry exists and only one-half the area must be examined. The parameter R is defined as the ratio of the two edges of the minimum rectangular area which must be examined to define

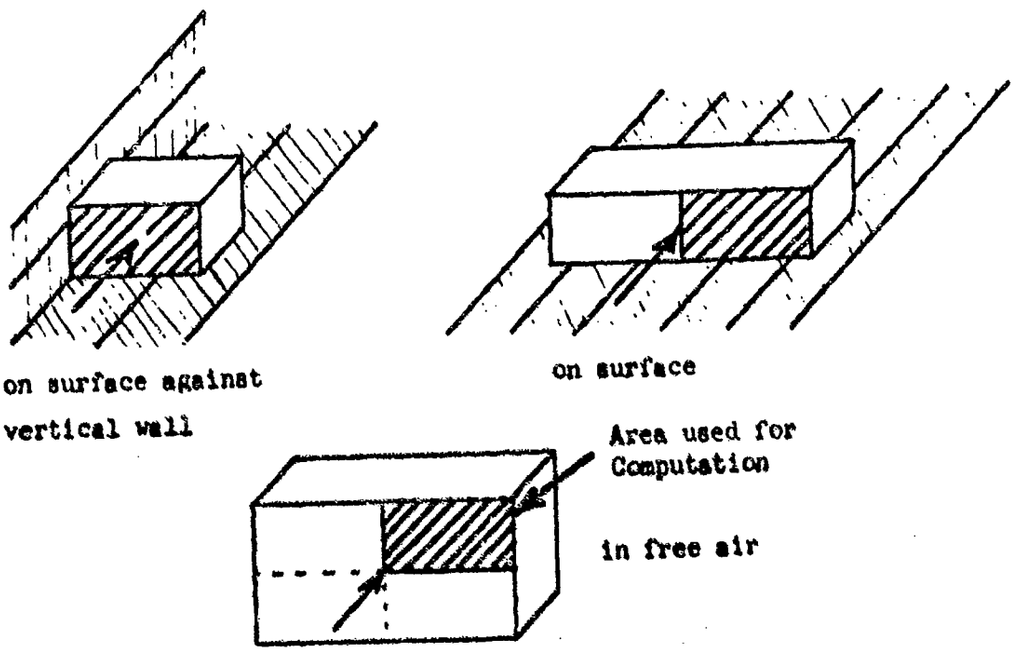

Figure 5 Minimum rectangular area which must be examined to determine loading on a front surface for several exposure conditions.

pressure loading over the entire front surface. The ratio is taken so that R is less than or equal to one. For the two-dimensional data obtained for the configurations shown in Figures 2B and 2D the value of R is zero. For the three-dimensional configurations shown in Figures 2A and 2C the value of R is essentially one.

It was assumed that the average pressure loading would vary from that for R = 0 to that for R = 1 in proportion to the value of R. In the fitted equations, then, the parameter R is inserted where a difference due to configuration occurs to produce a smooth variation with the value of R. The final form of the fitted equation for front-surface loading was Equation 1 with:

$$A = 0.265\ z^{-0.20}$$

$$B = 1.5R + (1 - R)\ (0.97 + e^{-0.177\ z^{0.37}}) \qquad (4)$$

$$P_R = 2\ P_s(4z + 7)/(z + 7)$$

$$P_L = P_{stag}$$

where: P_{stag} = stagnation overpressure on the front surface; which for Mach number less than one is:

$$P_{stag} = (P_s + P_A)\left[1 + \frac{5z^2}{7(z+1)(z+7)}\right]^{7/2} - P_A$$

P_s = incident shock overpressure

P_A = ambient atmospheric pressure

$z = P_s/P_A$

$$a_s = a_o\sqrt{\frac{(8z+7)(2z+7)}{7(7+6z)}}$$

a_o = sound velocity = $331.32\sqrt{\frac{T_A}{273.16}}$ m/s

T_A = ambient atmospheric temperature, degrees Kelvin

Figures 6 through 13 show the curves from Figures 3 and 4 compared with values calculated using Equation 1 with functions defined as shown in Equation 4.

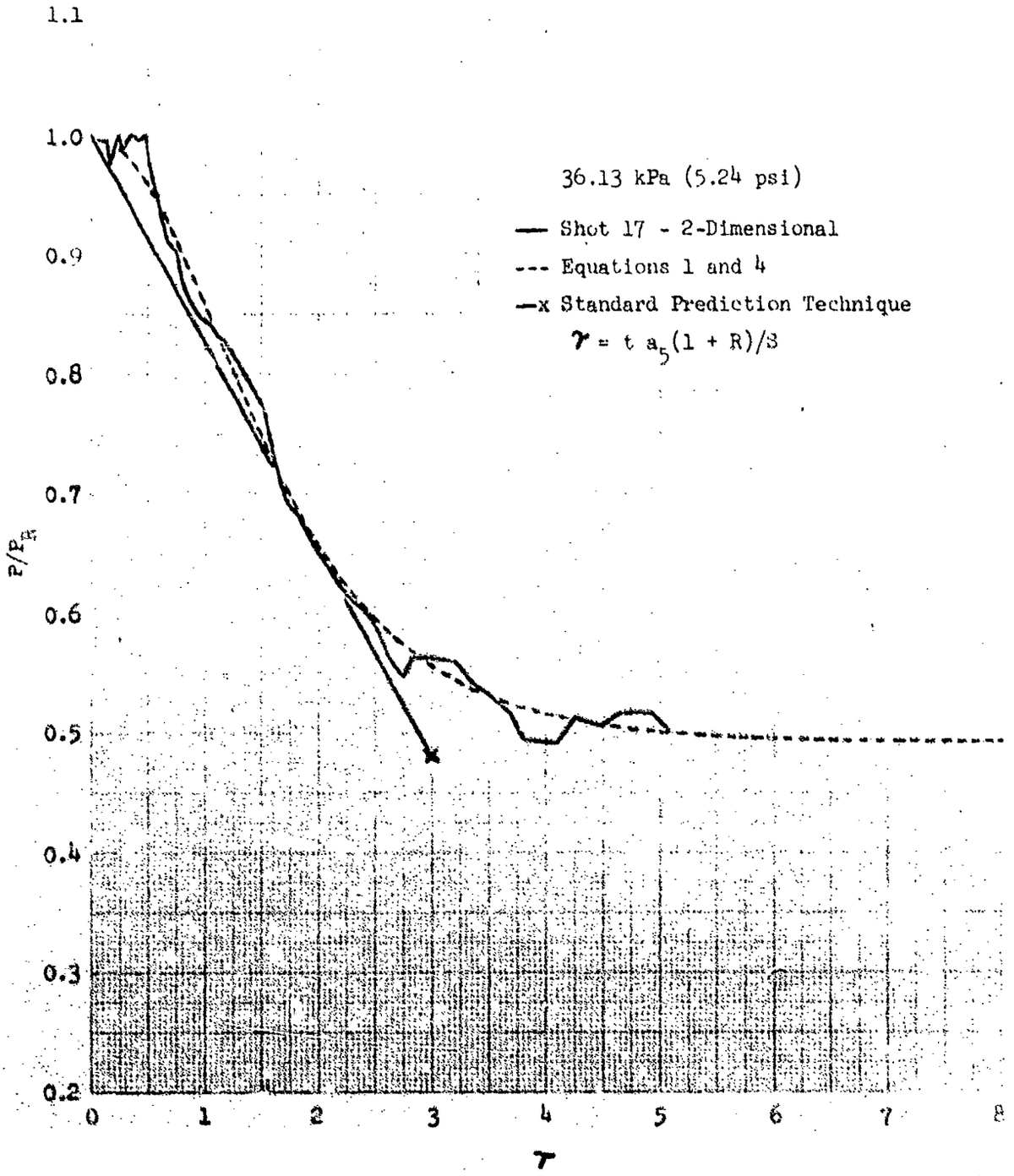

Figure 6 Average pressure ratio on the front face of the two-dimensional shock tube target compared with fitted equations and a standard prediction technique for an incident shock overpressure of 36.13 kPa (5.24 psi).

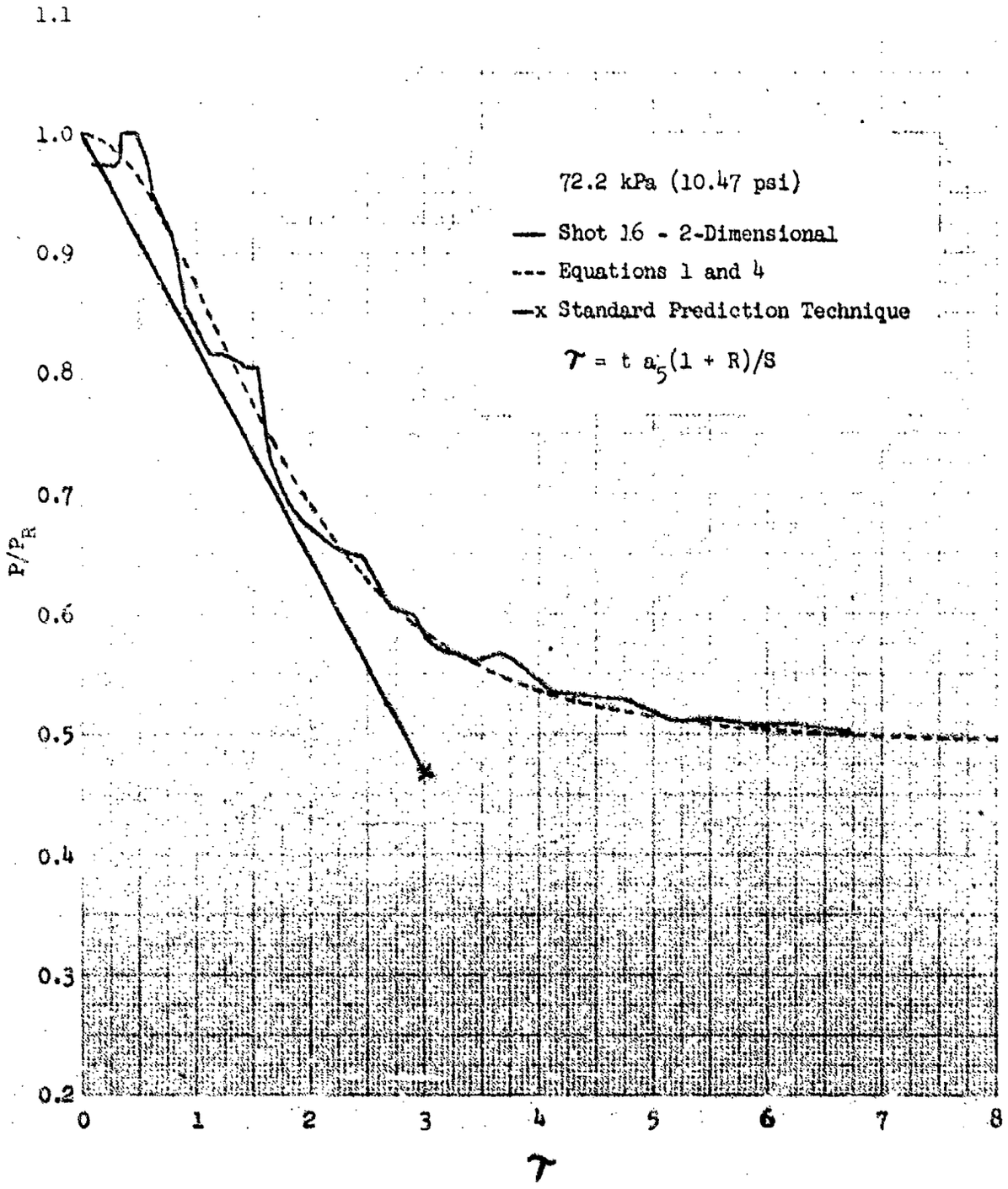

Figure 7 Average pressure ratio on the front face of the two-dimensional shock tube target compared with fitted equations and a standard prediction technique for an incident shock overpressure of 72.2 kPa (10.47 psi).

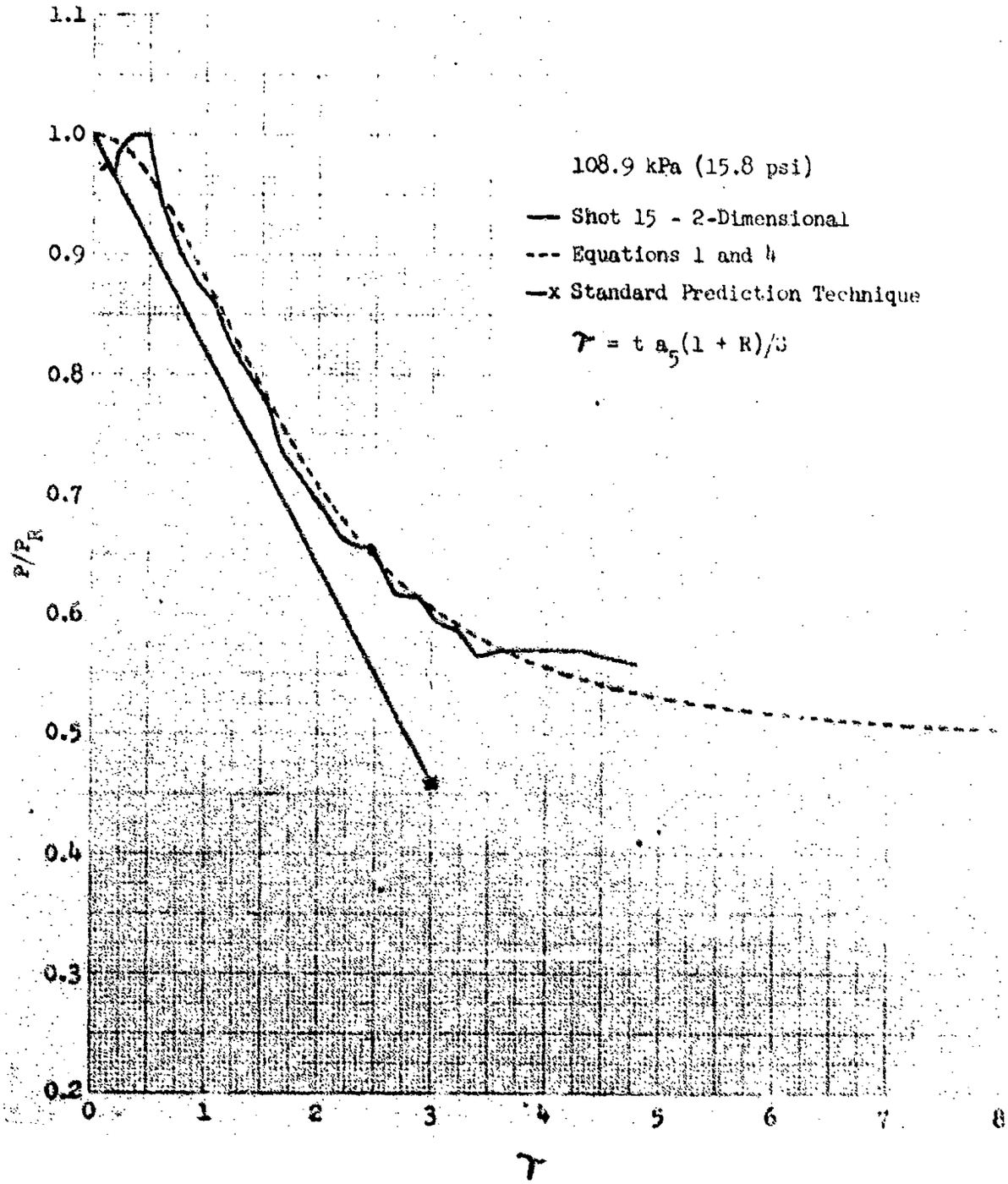

Figure 8 Average pressure ratio on the front face of the two-dimensional shock tube target compared with fitted equations and a standard prediction technique for an incident shock overpressure of 108.9 kPa (15.8 psi).

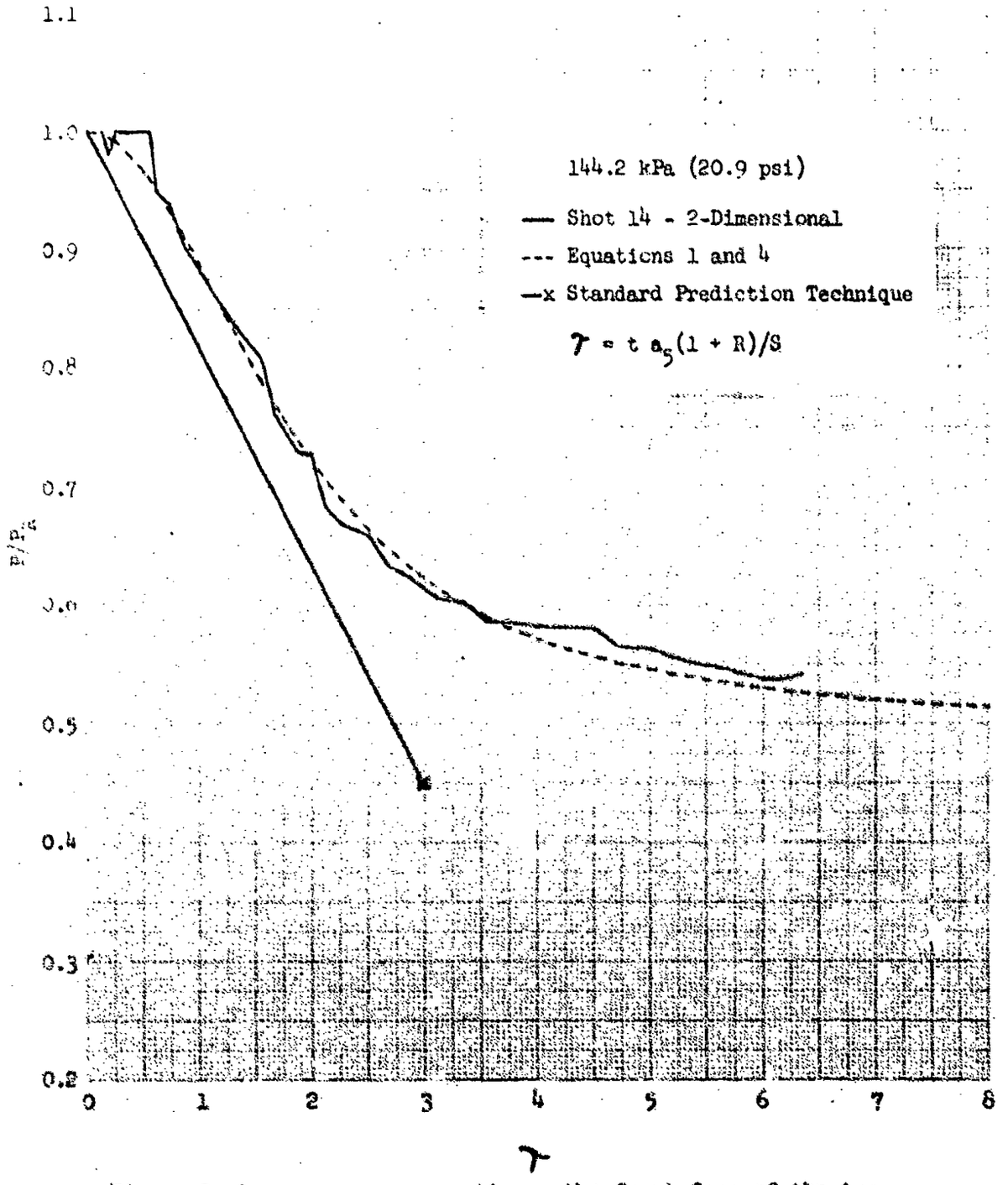

Figure 9 Average pressure ratio on the front face of the two-dimensional shock tube target compared with fitted equations and a standard prediction technique for an incident shock overpressure of 144.2 kPa (20.9 psi).

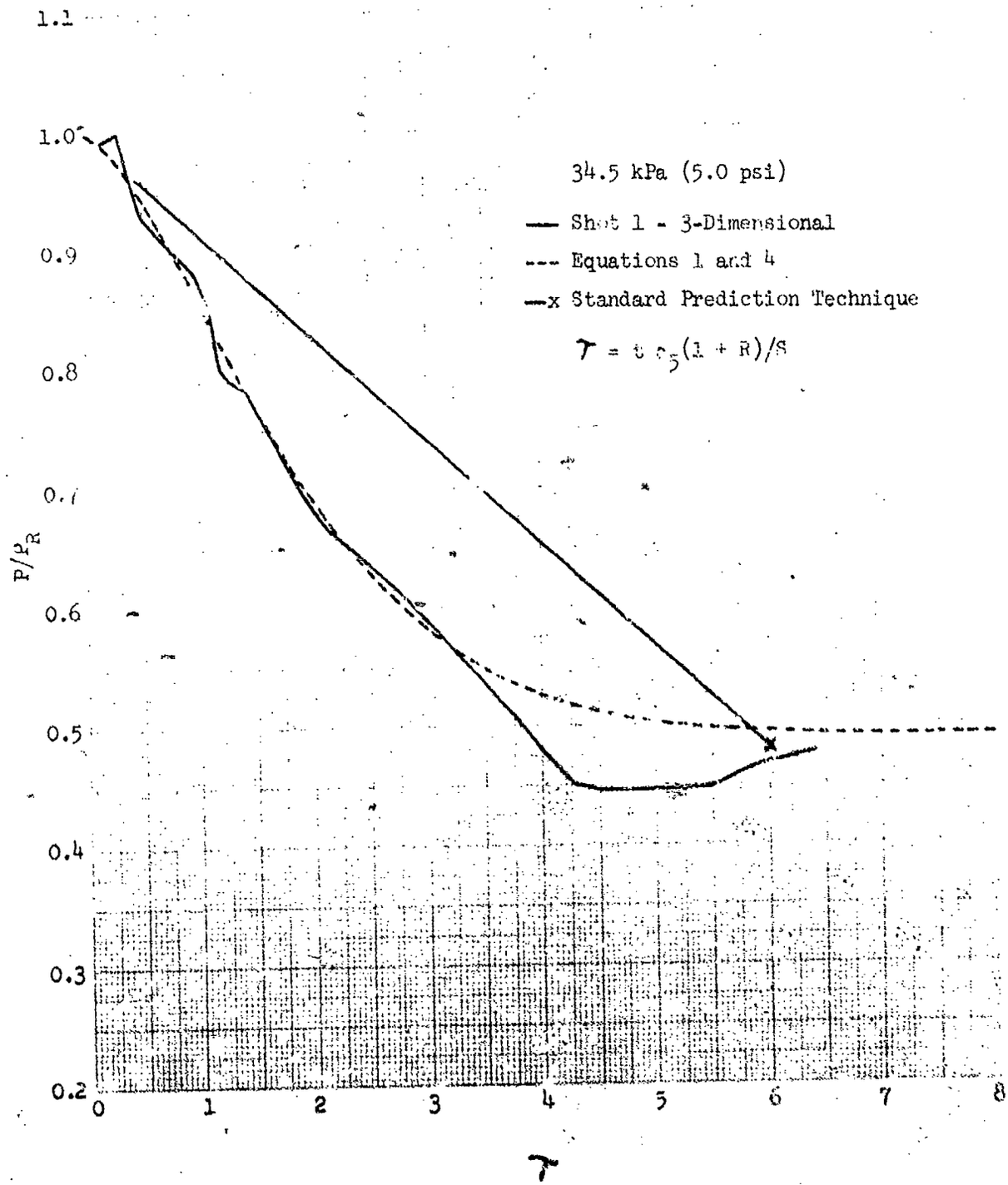

Figure 10 Average pressure ratio on the front face of the three-dimensional shock tube target compared with fitted equations and a standard prediction technique for an incident shock overpressure of 34.5 kPa (5.0 psi).

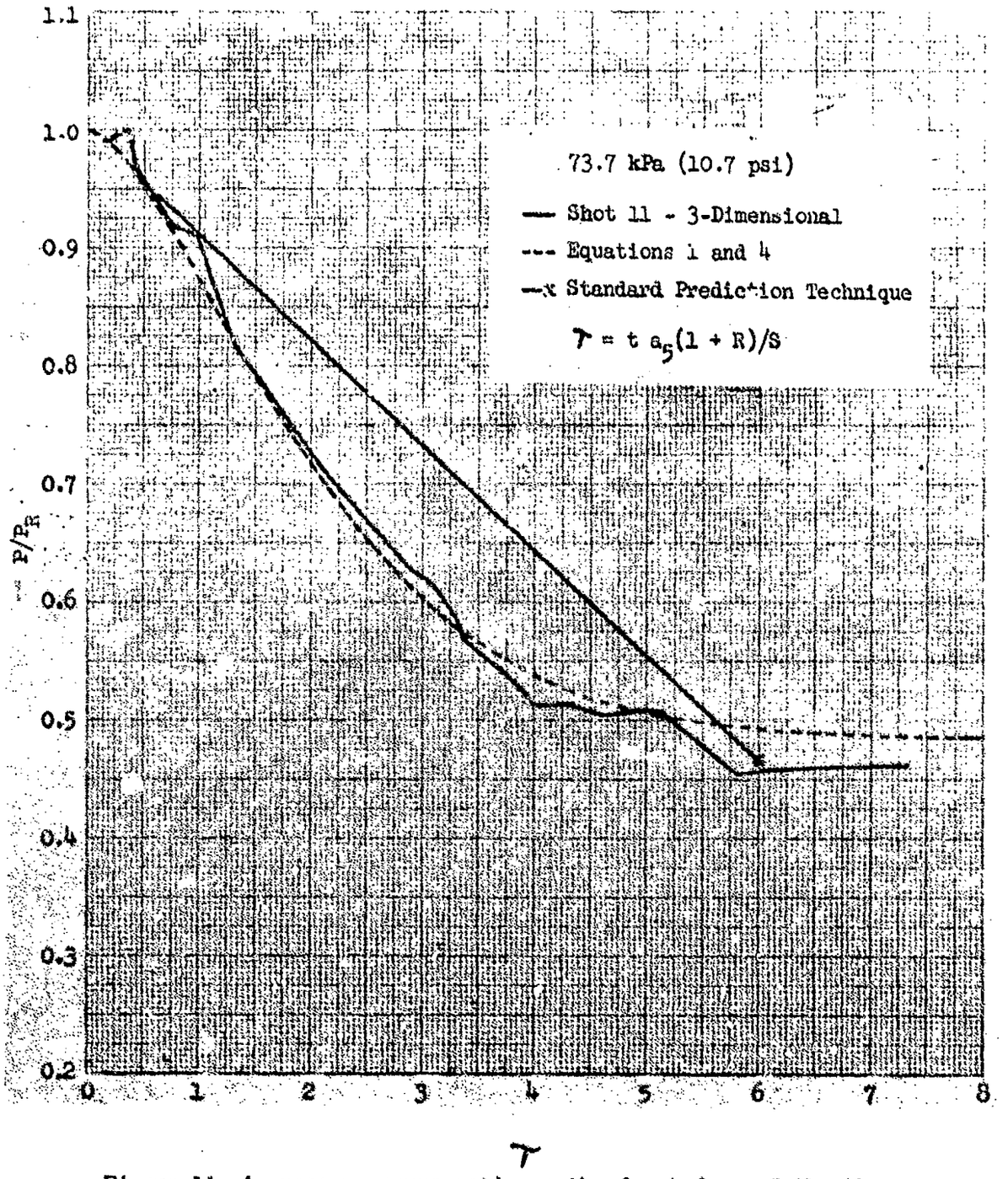

Figure 11 Average pressure ratio on the front face of the three-dimensional shock tube target compared with fitted equations and a standard prediction technique for an incident shock overpressure of 73.7 kPa (10.7 psi).

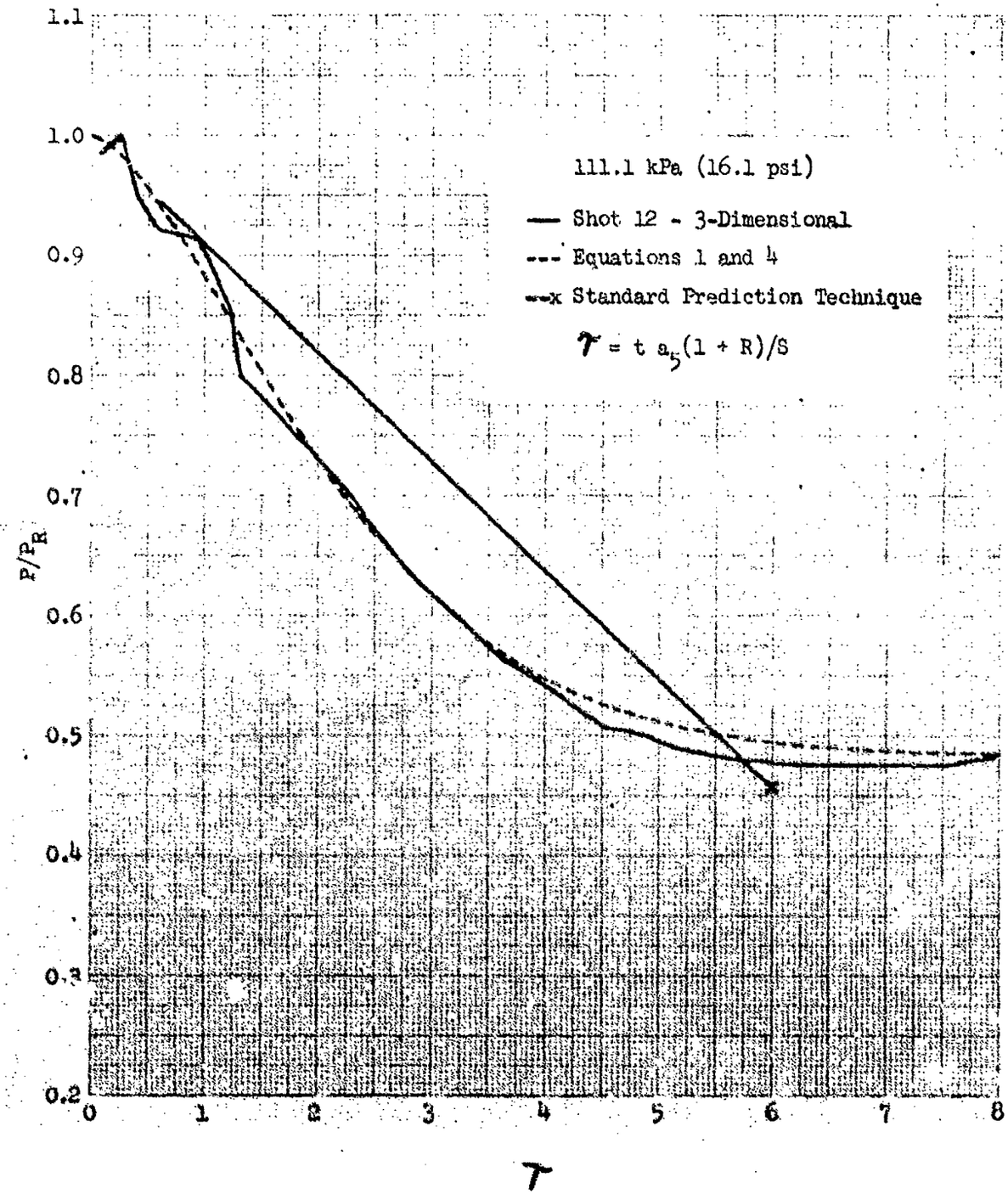

Figure 12 Average pressure ratio on the front face of the three-dimensional shock tube target compared with fitted equations and a standard prediction technique for an incident shock overpressure of 111.1 kPa (16.1 psi).

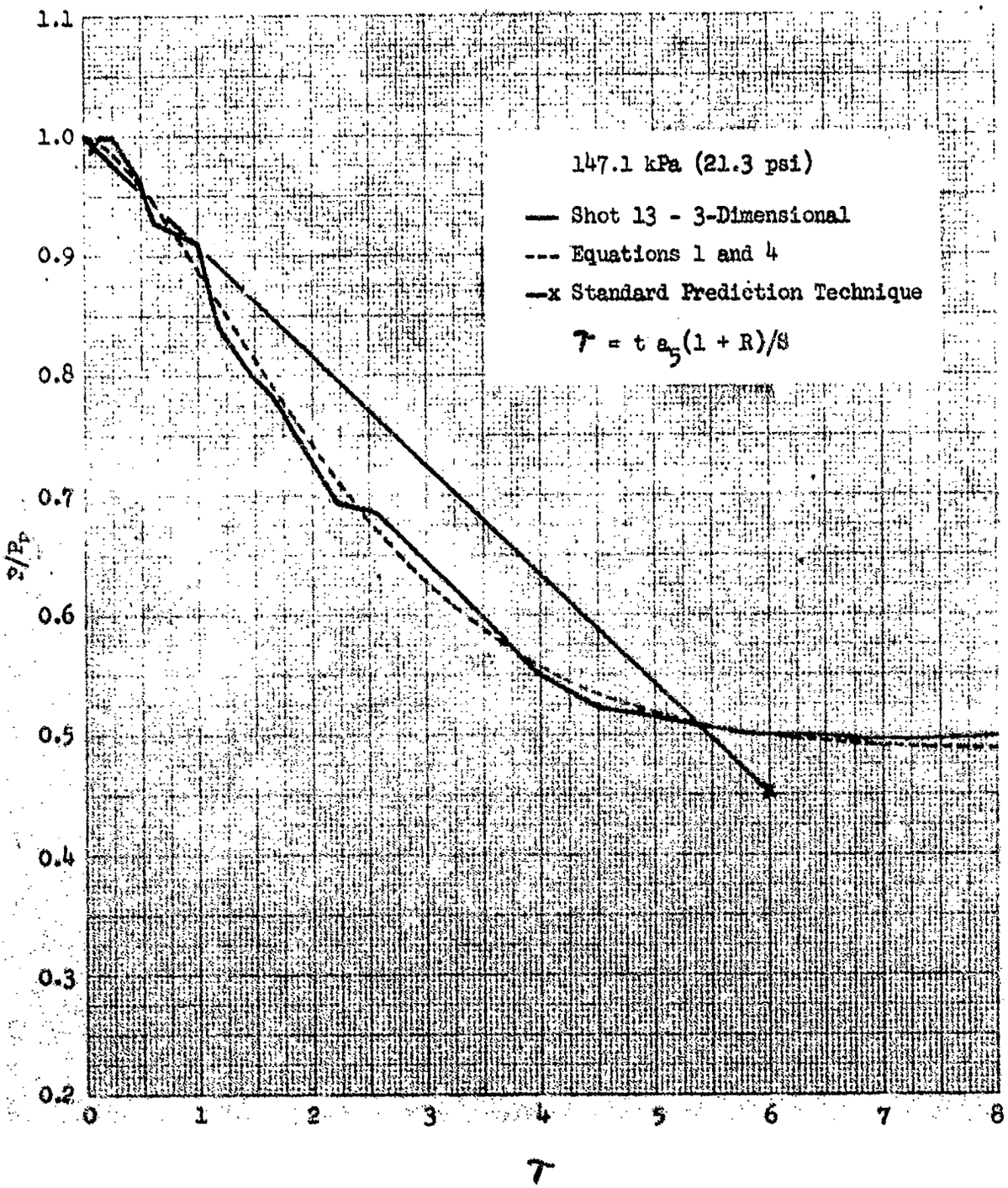

Figure 13 Average pressure ratio on the front face of the three-dimensional shock tube target compared with fitted equations and a standard prediction technique for an incident shock overpressure of 147.1 kPa (21.3 psi).

The quality of fit to the experimental data was judged by inspection rather than on statistical measures which would be provided by a least-squares fit of Equation 1 to the data. The fits developed are estimated to be within the range of error for gage records and the gage record averaging procedure.

Before performing the fits, the curves from Figures 3 and 4 were normalized so that the peak value corresponded to the peak reflected pressure. These experimental summed gage records should show an initial period of no decay which corresponds to the time for a rarefaction wave to reach the nearest gage from an edge. The actual average loading curve will begin to decay immediately.

The equation was fitted to data for overpressures ranging from 34.5 to 138 kPa (5 to 20 psi). The equation can be used outside this range, say from 13.8 to 345 kPa (2 to 50 psi), but with less confidence. Figure 14 shows curves calculated using Equation 1 with functions as defined in Equation 4 for 13.8, 34.47, 137.9, and 344.7 kPa (2, 5, 20, and 50 psi) for P_A = 101.325 kPa (14.696 psi) and T_A = 15°C and R = 0.5, and γ = 1.4.

B. Comparisons with Other Shock Tube Data

Reference 6 presents shock tube data on front-surface loading obtained on a target with R = 1.0, corresponding to the three-dimensional configuration, for overpressures of 22, 40, 62, and 100 kPa (3.2, 5.8, 9.0, and 14.5 psi) at an average P_A of 102 kPa (14.8 psi). The target was 50.8 mm (2 in.) high, 101.6 mm (4 in.) wide and 50.8 mm (2 in.) deep. Five gages were located on the front face. The individual gages were recorded separately. The records were read and the values combined to form the average front-surface pressure. The records show a finite rise time, and the peak values do not correspond to the theoretical values of peak reflected pressures appropriate for the values quoted for the incident overpressure. However, it is not clear that accuracy of the average pressure at later times would be improved by normalizing the records so that the peak values shown in Figures 21-24 of Reference 6 would correspond to the theoretical peak reflected pressures. These curves were transformed to plots of $P_{average}/P_R$ versus τ without attempting any normalization.

The transformed curves are shown in Figures 15 and 16. The dashed curves were calculated using Equation 1 with functions as defined in Equation 4. The agreement between the predicted curves and the data curves is best for the lowest incident shock overpressure. Agreement

[6] *C. N. Kingery and J. H. Keefer, "Air Blast Loading on a Three-Dimensional Structure," BRL Report 952, AFSWP Report 813, July 1955.* (AD #78562)

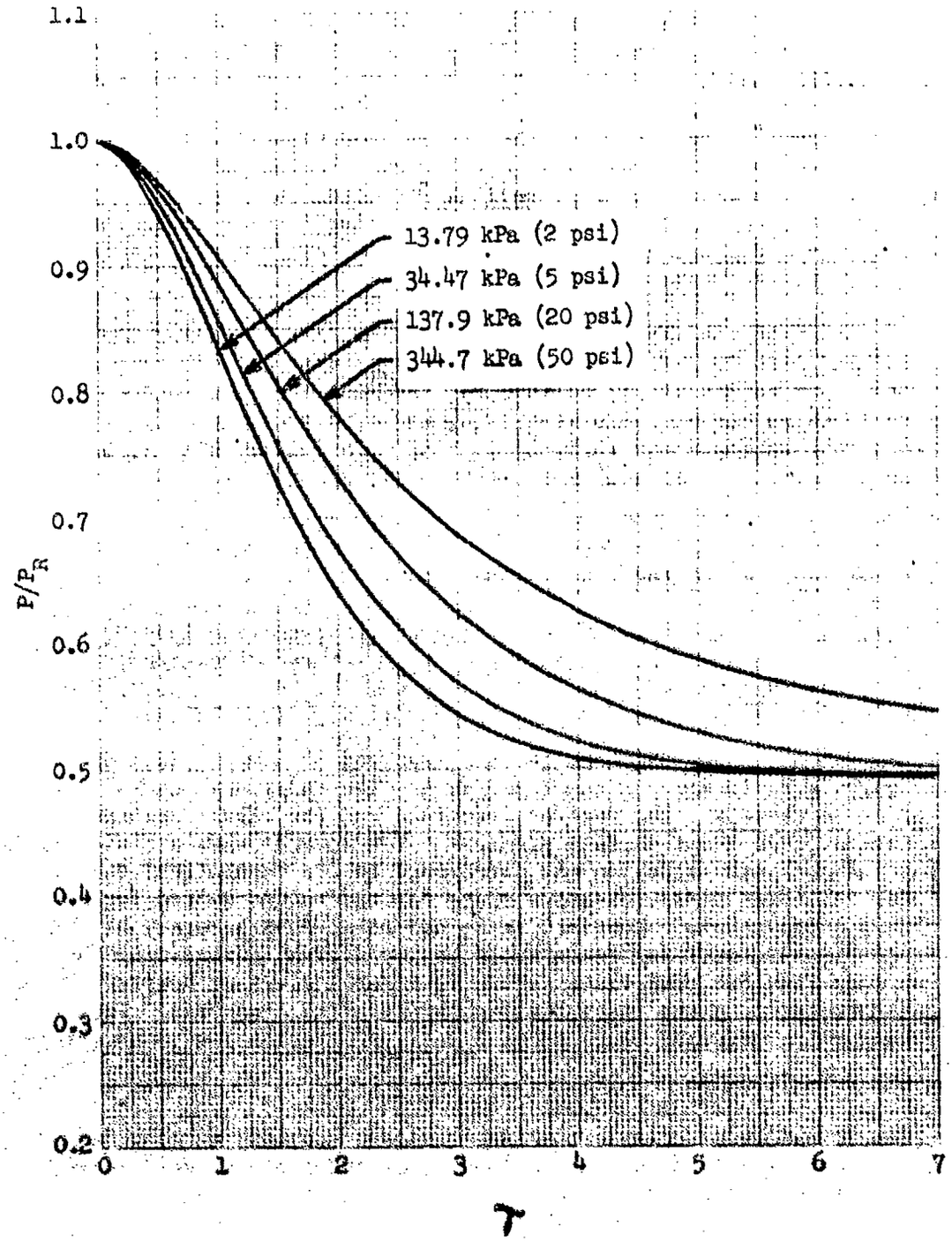

Figure 14 Average pressure ratios calculated using Equations 1 and 4 for 13.79, 34.47, 137.9, and 344.7 kPa (2, 5, 20, and 50 psi) for P_A = 101.325 kPa (14.696 psi) and T_A = 288.15 degrees Kelvin and R = 0.5.

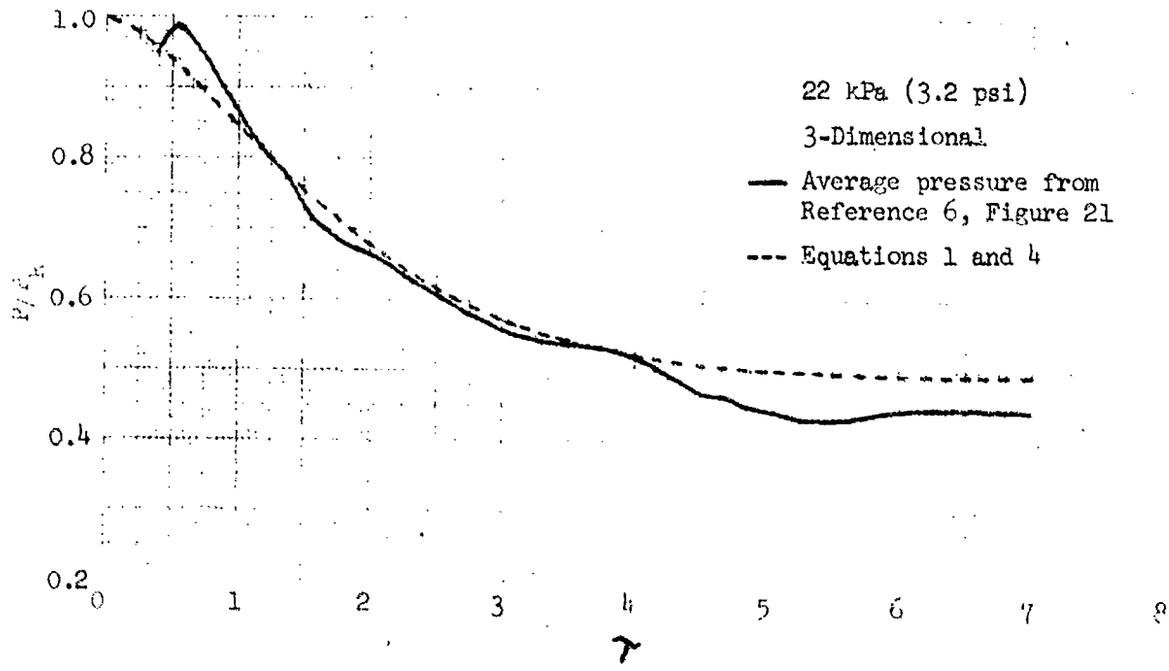

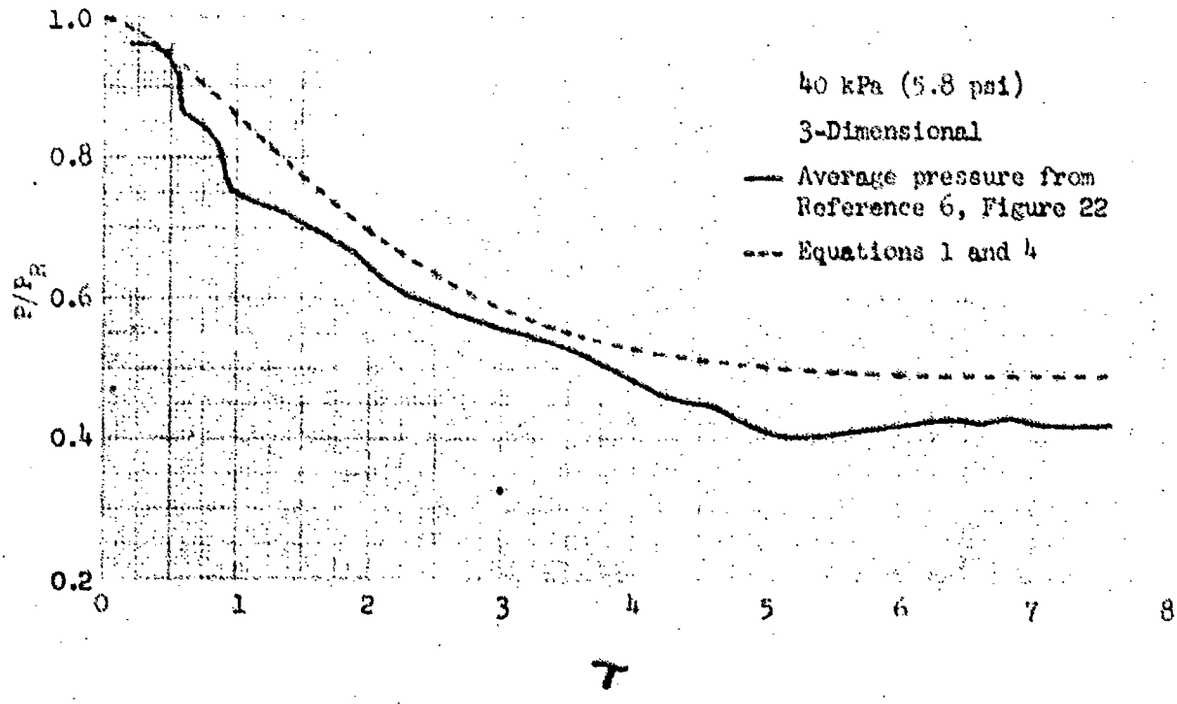

Figure 15 Comparison of Equations 1 and 4 with average pressure ratios on the front face of the shock tube target of Reference 6. Incident shock overpressures were 22 and 40 kPa (3.2 and 5.8 psi) and R = 1.0.

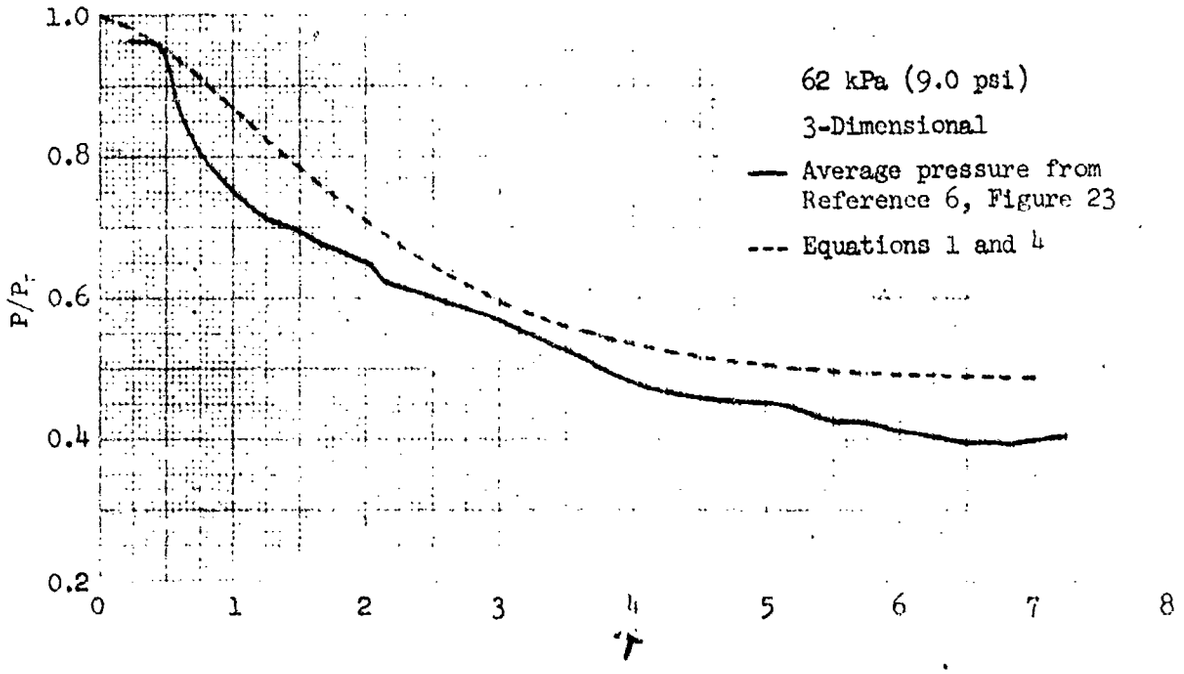

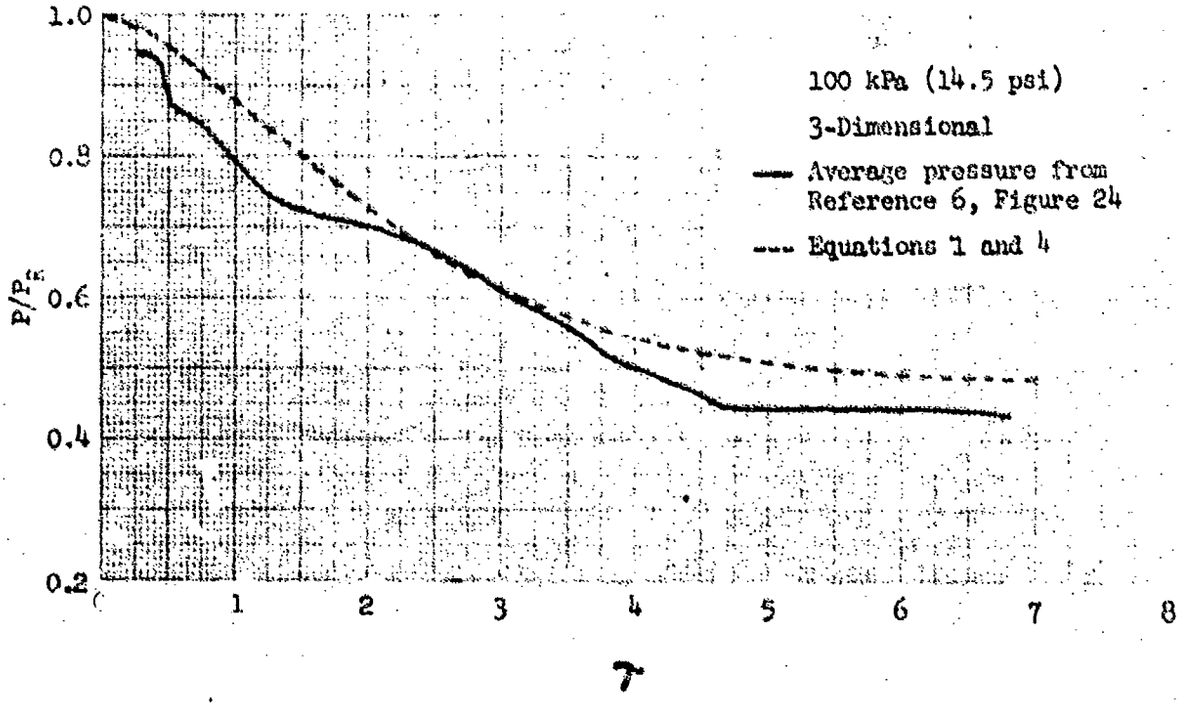

Figure 16 Comparison of Equations 1 and 4 with average pressure ratios on the front face of the shock tube target of Reference 6. Incident shock overpressures were 62 and 100 kPa (9.0 and 14.5 psi) and R = 1.0.

would indeed be improved if normalization of the shock tube data to the theoretical values of peak reflected pressure were justified. The general shape of the experimental curves seems to correspond to the predicted curves. The data indicate a decay to an overpressure below the stagnation pressure.

C. Comparison with a Three-Dimensional Hydrocode Calculation

In Reference 7, Lottero presents the results of a three-dimensional hydrocode calculation of the loading developed on an S-280 Electrical Equipment Shelter by a 34.475 kPa (5 psi) shock wave. The shock wave was assumed to have no decay in pressure behind the shock front, and to strike the side of the shelter at normal incidence. The calculation was made by R. A. Gentry, et al., at the Los Alamos Scientific Laboratory using the hydrocode BAAL. The calculation was made in the same fashion as that reported by Gentry in Reference 5.

Figure 17 shows a plot of predictions made using Equations 1 and 4 compared with the average pressure computed from the hydrocode results. The ratio of $P_{average}/P_R$ is shown plotted versus time. Values of the parameters used in Equation 4 were $P_{stag}/P_R = 0.4904$, $S = 1.81$ metres, $R = 0.8584$, $a_5 = 369.62$ m/s, and $z = 0.3402$.

The hydrocode data indicate an initial decay to a pressure value less than the stagnation pressure limit of Equation 1 with functions as defined in Equation 4. A pressure limit somewhat less than stagnation pressure is physically reasonable, since there will be some flow across the front-surface area and near the edges the pressure will not be at the full stagnation value. The agreement between the predicted curve and the hydrocode data points seems satisfactory.

D. Comparison with Standard Prediction Techniques

In Reference 3 the average pressure on the front surface of a target is presented as decaying from the peak reflected pressure to a value $P_s + 0.85\ P_q$, where P_s is the overpressure and P_q is the dynamic pressure in the blast wave. The decay is approximated by a straight line and occurs in the time $t_* = 3\ S/a_5$. This time corresponds to $\tau = 3$ for the two-dimensional configuration where $R = 0$ and to $\tau = 6$ for the three-dimensional configuration where $R = 1$. In Figures 6 through 13 the predictions made using this technique are shown by the straight lines terminating at an X. The disagreement is particularly large for the three-dimensional configuration. The primary purpose of the work by Taylor[2] was to point out this disagreement and to emphasize that the standard prediction techniques were not very good when applied to the three-dimensional configuration.

---

[7] *R. E. Lottero, "Computational Predictions of Shock Diffraction Loading on an S-280 Electrical Equipment Shelter," BRL Memorandum Report 2599, March 1976.* (AD #A023804)

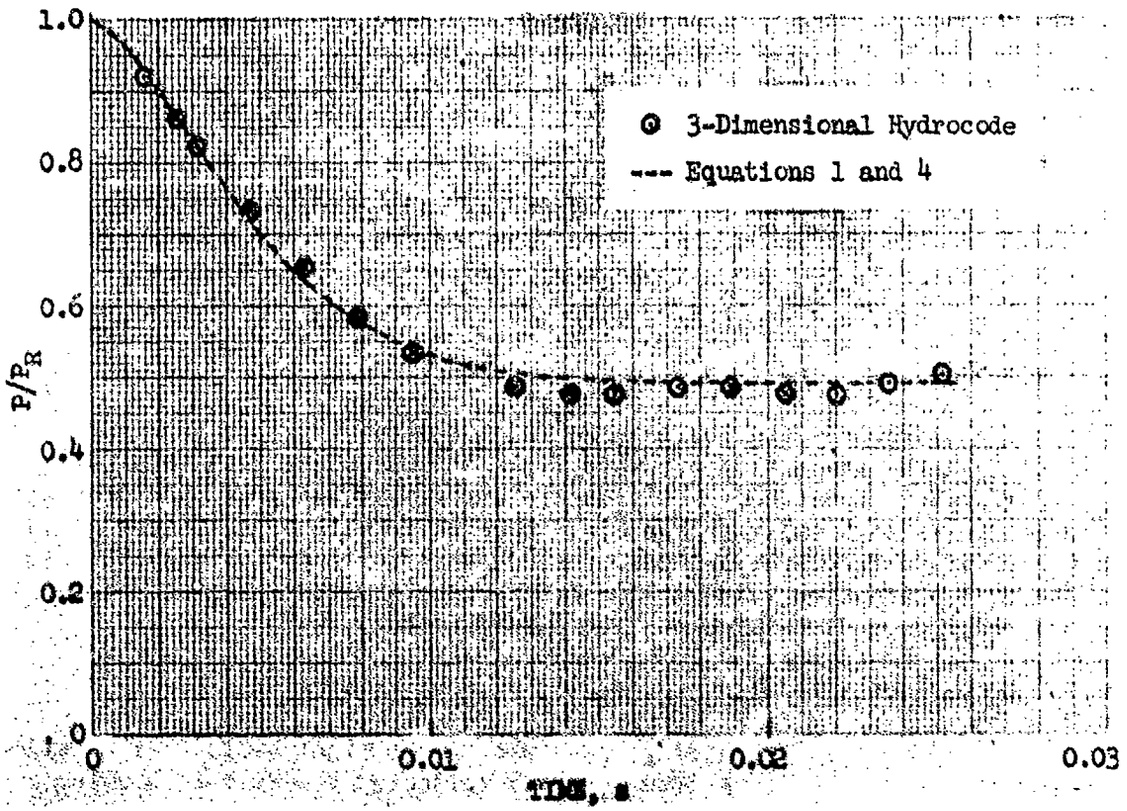

Figure 17 Comparison of average pressure ratio computed[7] for an S-280 Electrical Equipment Shelter using a three-dimensional hydrocode (BAAL) with Equations 1 and 4 for an incident shock overpressure of 34.47 kPa (5 psi).

E. Modification to Account for the Decay of the Incident Blast Wave

The data obtained by Taylor[2] apply for a shock wave with no pressure decay behind the shock front, which corresponds to a blast wave from an infinitely large explosion. To account for the pressure decay which occurs in a real blast wave, the pressures predicted by Equation 1 are reduced in proportion to the reduction in P_{stag} with time. This provides only an approximation to the correct pressure, since the reflected pressure is a non-linear function of the incident shock overpressure waveform. However, the correct function is not available. A treatment of non-linear shock wave reflection theory in one-dimensional form is given in Reference 8, and is quite complex, even for one-dimensional flow.

If this procedure is incorporated into Equation 1 to account for the decay with time of the incident shock overpressure, the prediction equation becomes as follows:

$$P(t) = \left[P_R \left(1 - \frac{P_{stag}}{P_R}\right) e^{-A\tau^B} + P_{stag} \right] \cdot \frac{P_{stag}(t)}{P_{stag}} \qquad (5)$$

where: $P(t)$ = average front-surface overpressure at time t

$P_{stag}(t)$ = stagnation overpressure in the blast wave at time t

$$= (P_s(t) + P_A) \left[1 + \frac{2\, P_q(t)}{7(P_s(t) + P_A)} \right]^{7/2} - P_A$$

$P_s(t)$ = overpressure in the blast wave at time t

P_{stag} = stagnation overpressure corresponding to peak incident overpressure P_s.

F. An Alternative Fit to the Average Front-Surface Overpressure

In the course of using Equation 1 for predictions it was noted that predicted curves for the extreme ends of the overpressure range of interest (13 to 345 kPa, or 2 to 50 psi) did not differ very much in initial shape when plotted as $P_{average}/P_R$ versus time. This result suggested examination of the data in terms of a time normalization with no dependence on overpressure, such as $\tau_* = t\, a_o (1 + R)/S$, where a_o is the sound velocity in the undisturbed air.

---

[8] *R. E. Shear and R. C. Makino, "A Non-Linear Shock Wave Reflection Theory," BRL Report 1361, January 1967 (AD 649946).*

Figures 18 and 19 show the two and three-dimensional data for $P_{average}/P_R$ plotted versus τ_*. The correspondence is such that no attempt was made to maintain the separate identity of the curves in the initial part of the plots. There is no indication of a consistent variation with overpressure level until most of the pressure decay has occurred.

Equations of the same basic form as Equation 1 were fitted to the data. For the two-dimensional case, R = 0, the results for the functions A and B were:

$$A = 0.388$$

$$B = 1.13z^{-0.3} + 0.026z^{0.93}\,(\tau-6)^2 \qquad (6)$$

$$P_L = P_{stag}$$

where $\tau = \tau_* = t\,a_o\,(1 + R)/S$, and other quantities have been defined for Equations 1 and 4.

For the three-dimensional data the fit was made neglecting the apparent variation in the limiting pressure at late times. The stagnation pressure was used as the limit to simplify joining the resulting equation with Equation 6 to obtain one equation applying for all values of R between 0 and 1. The results for A and B for the three-dimensional configuration were:

$$A = 0.346$$

$$B = 1.54 + 0.1\,(\tau-2.3)^2 \qquad (7)$$

$$P_L = P_{stag}$$

$$\tau = \tau_*$$

The final functions combining the results of both fittings are:

$$A = 0.388\,(1-R) + 0.346\,R$$

$$B = (1-R)\,[1.13z^{-0.3} + 0.026z^{0.93}\,(\tau-6)^2] + R\,[1.54 + 0.1\,(\tau-2.3)^2] \qquad (8)$$

$$P_L = P_{stag}$$

$$\tau = \tau_*$$

Figures 20 through 27 show the curves calculated from Equation 1 with functions as defined in Equation 9 compared with the experimental curves. It is clear that the resulting curves represent reasonable fits. Equation 1 can be used with functions as defined by either Equation 4 or Equation 8 in the range from 34.5 to 138 kPa (5 to 20 psi) with no significant difference in the result.

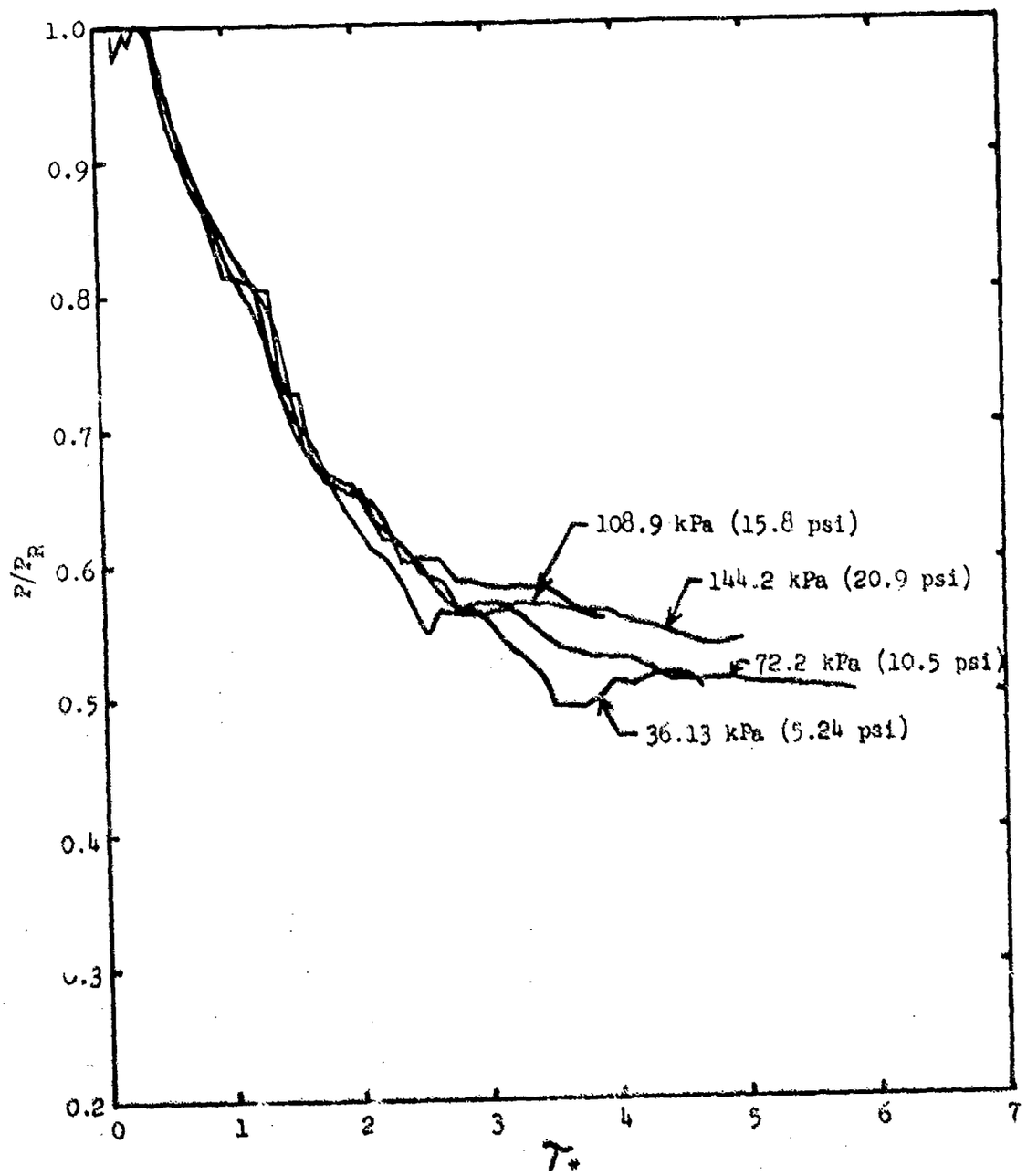

Figure 18 Average front surface pressure ratios of the two-dimensional shock tube target of Reference 2 plotted versus $\tau_* = t\, a_0(1 + R)/S$.

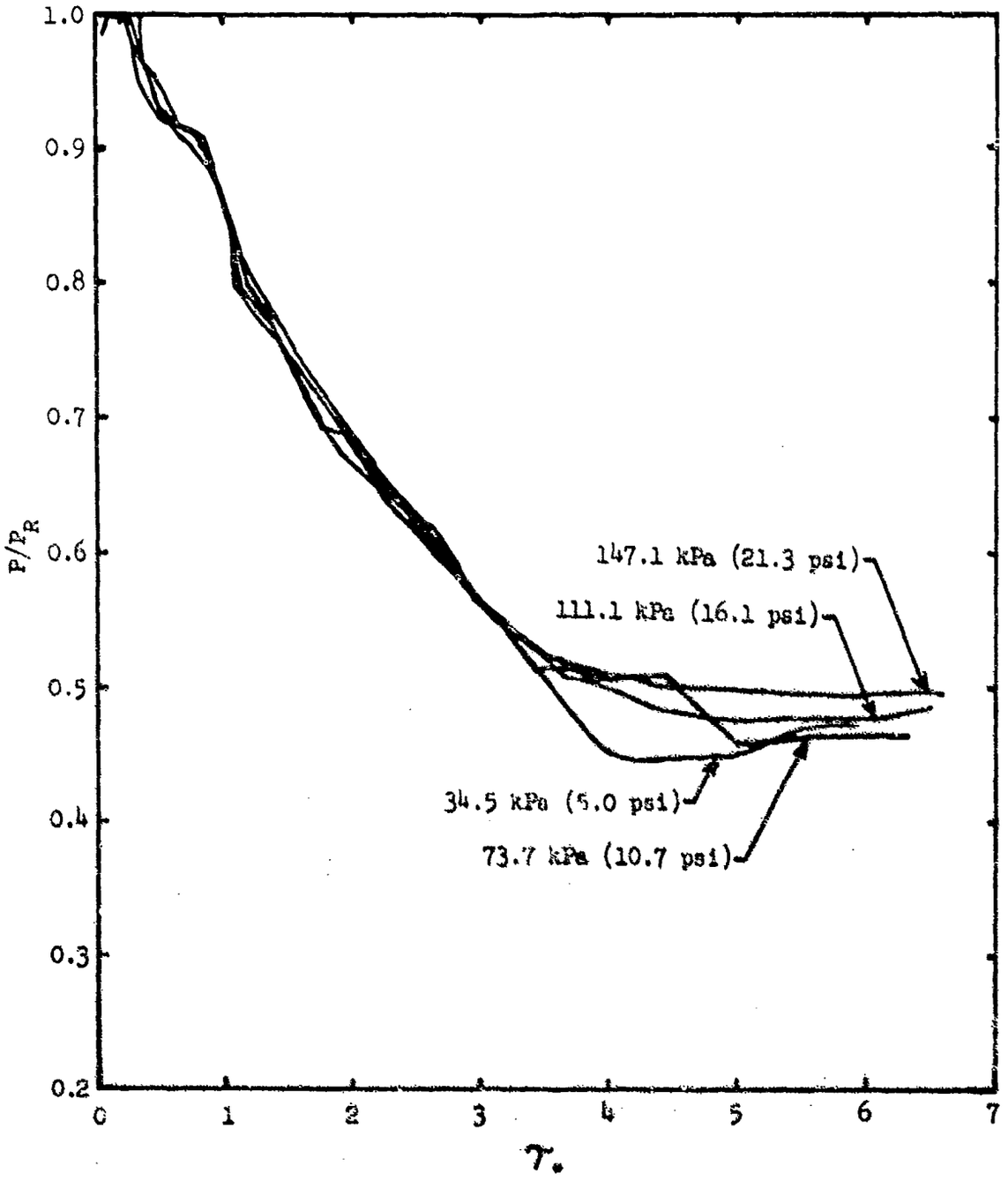

Figure 19 Average front surface pressure ratios of the three-dimensional shock tube target of Reference 2 plotted versus $\tau_* = t\, a_o(1 + R)/S$.

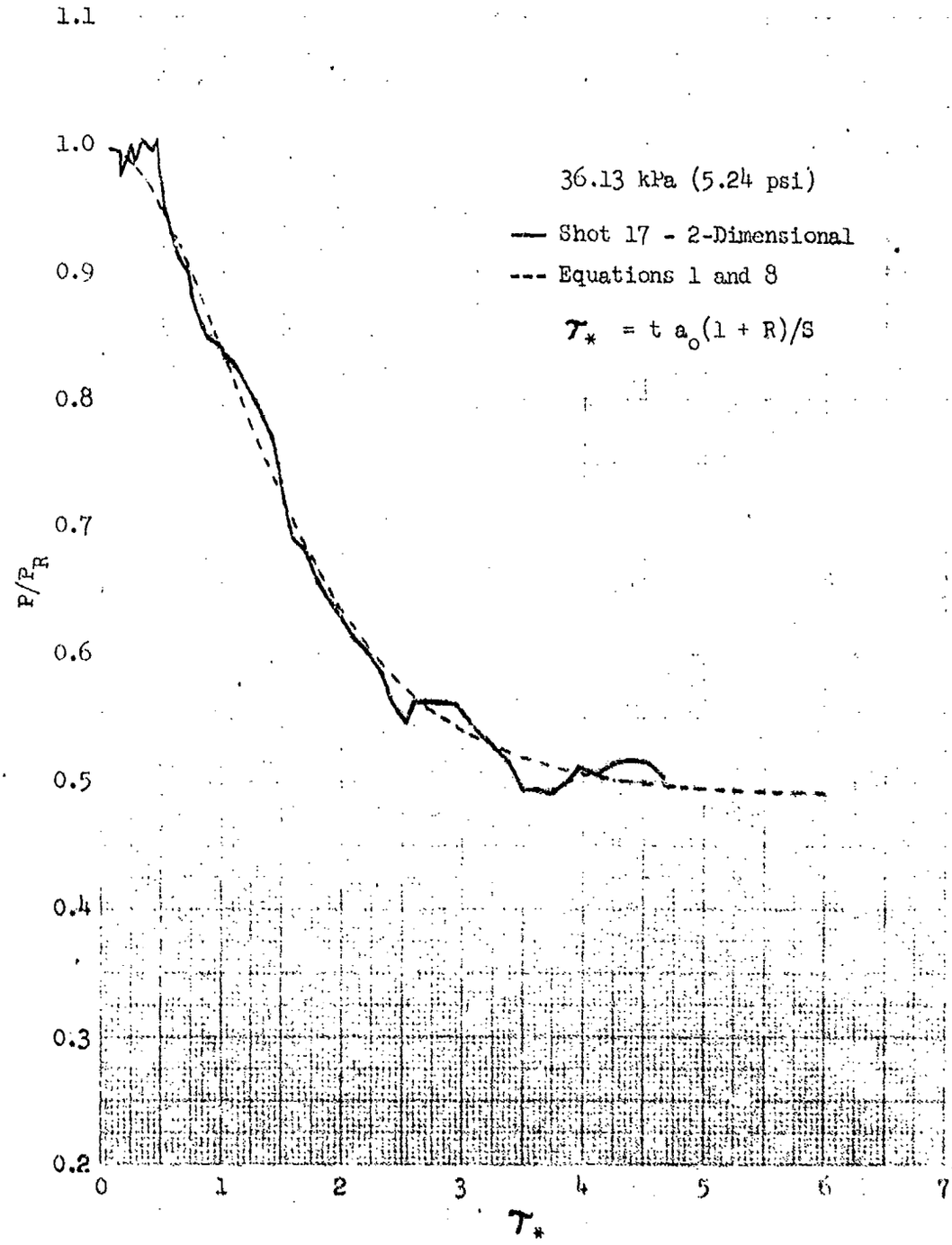

Figure 20 Average front surface pressure ratio of the two-dimensional shock tube target for an incident shock overpressure of 36.13 kPa (5.24 psi) plotted versus $\tau_* = t\, a_o(1 + R)/S$.

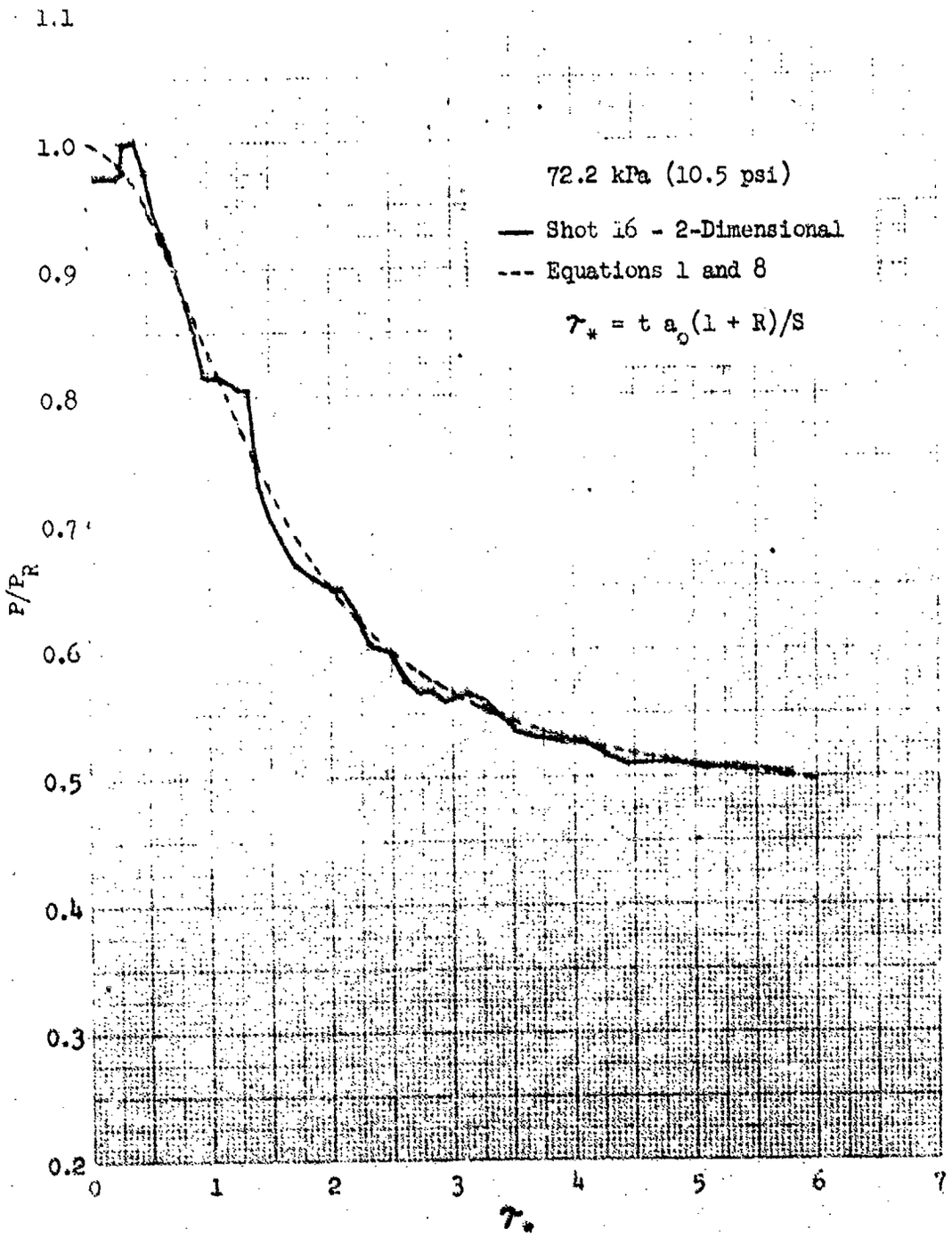

Figure 21 Average front surface pressure ratio of the two-dimensional shock tube target for an incident shock overpressure of 72.2 kPa (10.5 psi) plotted versus $\tau_* = t\, a_o(1 + R)/S$.

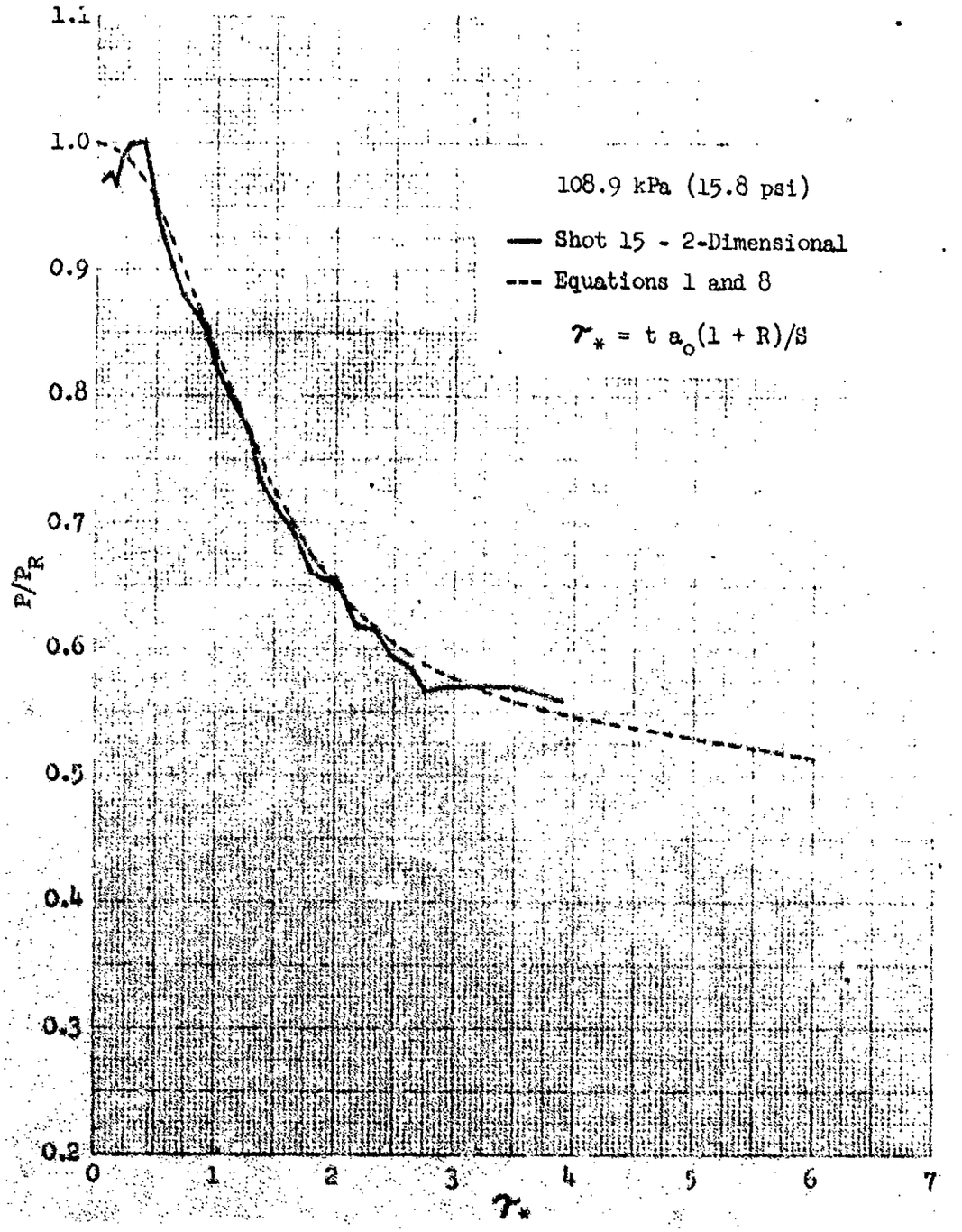

Figure 22 Average front surface pressure ratio of the two-dimensional shock tube target for an incident shock overpressure of 108.9 kPa (15.8 psi) plotted versus $\tau_* = t\, a_o(1 + R)/S$.

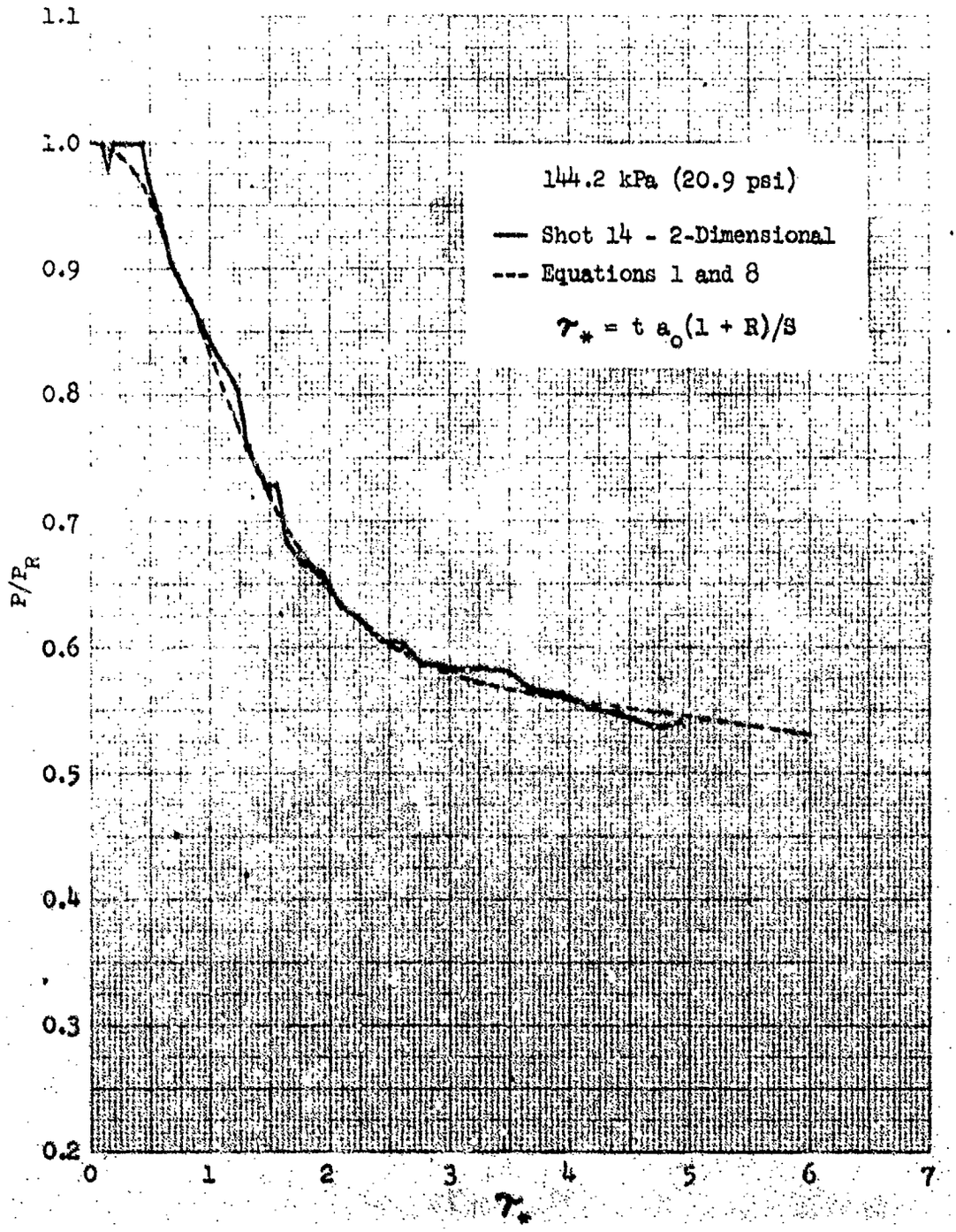

Figure 23 Average front surface pressure ratio of the two-dimensional shock tube target for an incident shock overpressure of 144.2 kPa (20.9 psi) plotted versus $\tau_* = t\, a_o(1 + R)/S$.

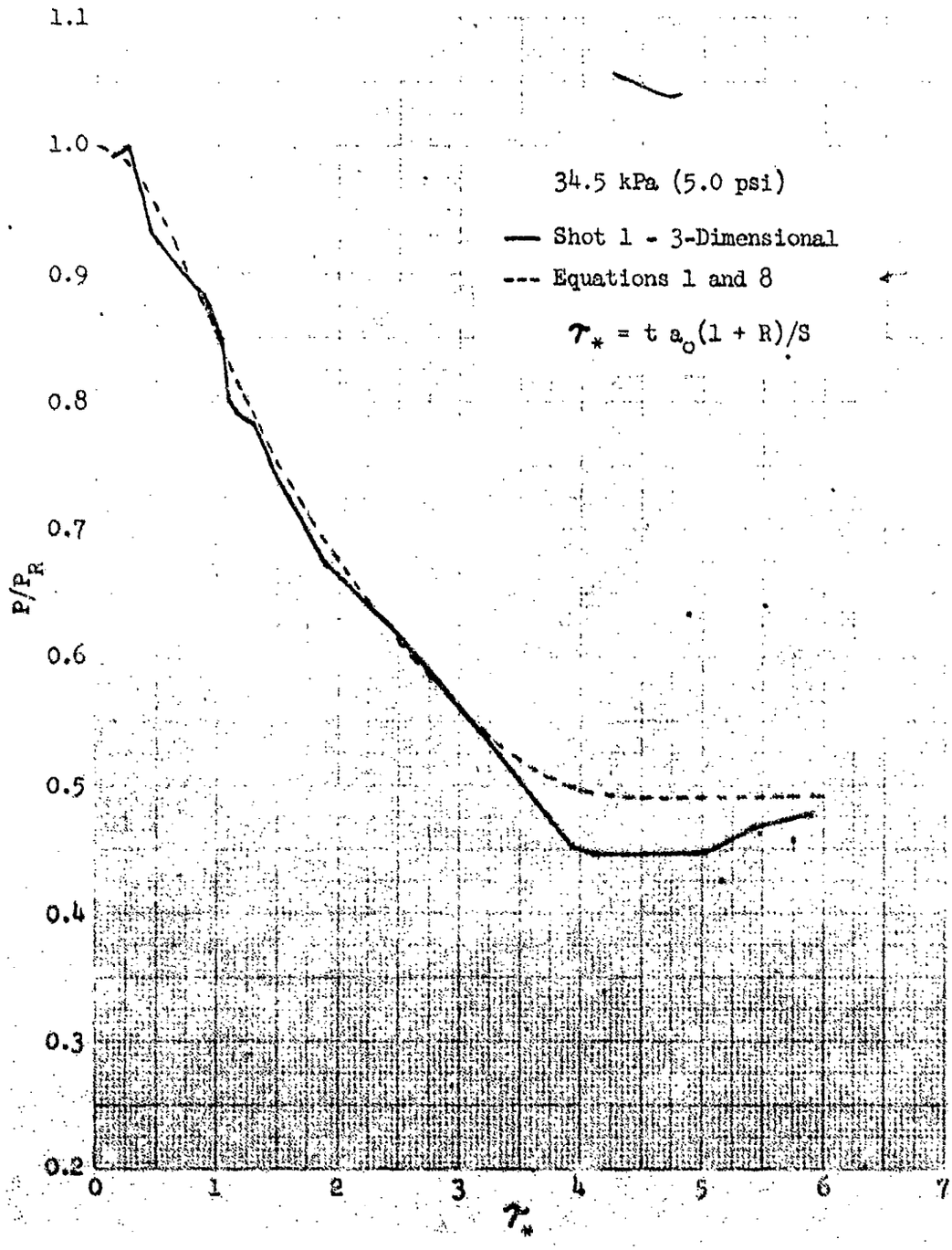

Figure 24 Average front surface pressure ratio of the three-dimensional shock tube target for an incident shock overpressure of 34.5 kPa (5.0 psi) plotted versus $\tau_* = t\, a_o(1 + R)/S$.

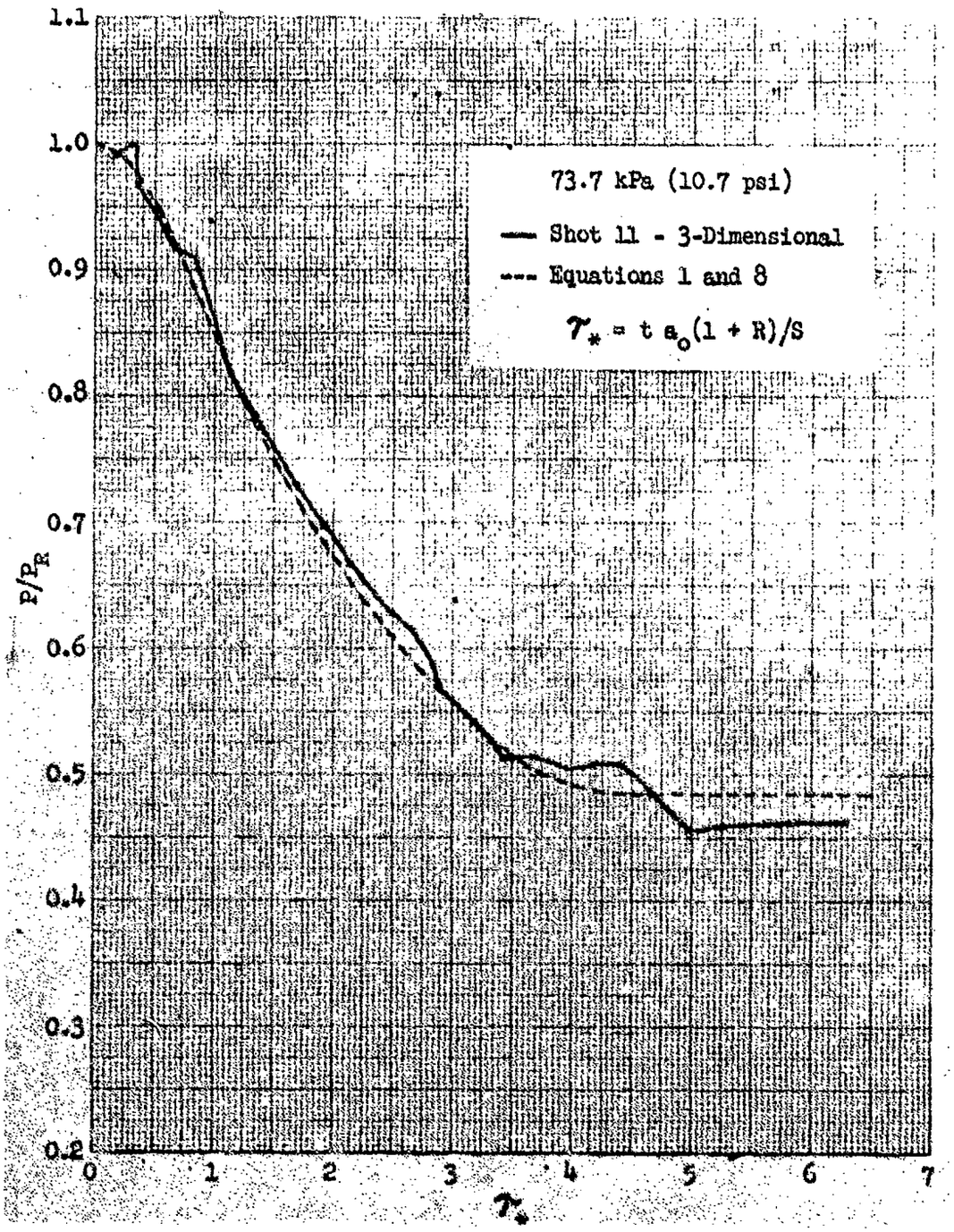

Figure 25 Average front surface pressure ratio of the three-dimensional shock tube target for an incident shock overpressure of 73.7 kPa (10.7 psi) plotted versus $\tau_* = t\, a_o(1 + R)/S$.

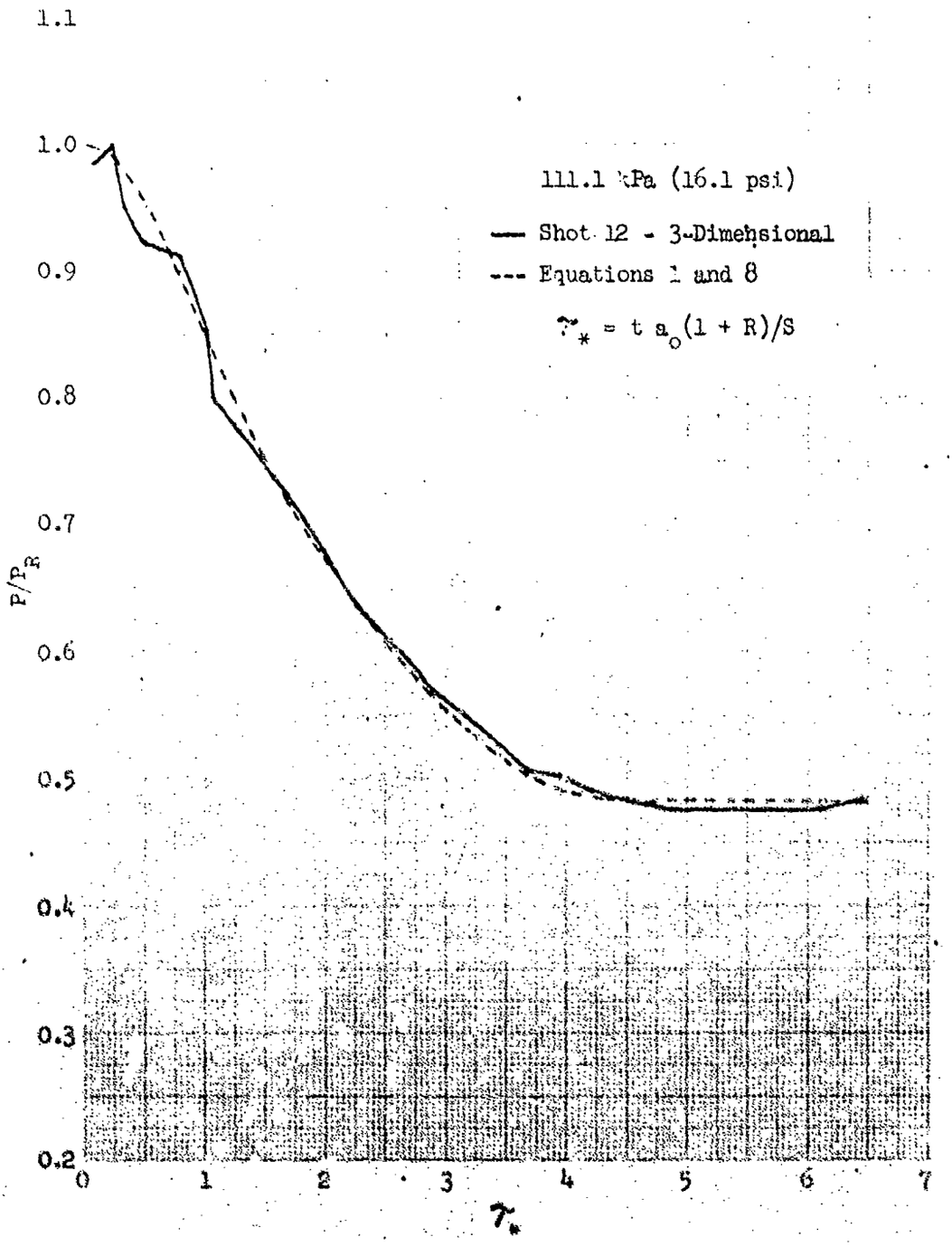

Figure 26 Average front surface pressure ratio of the three-dimensional shock tube target for an incident shock overpressure of 111.1 kPa (16.1 psi) plotted versus $\tau_* = t\, a_o(1 + R)/S$.

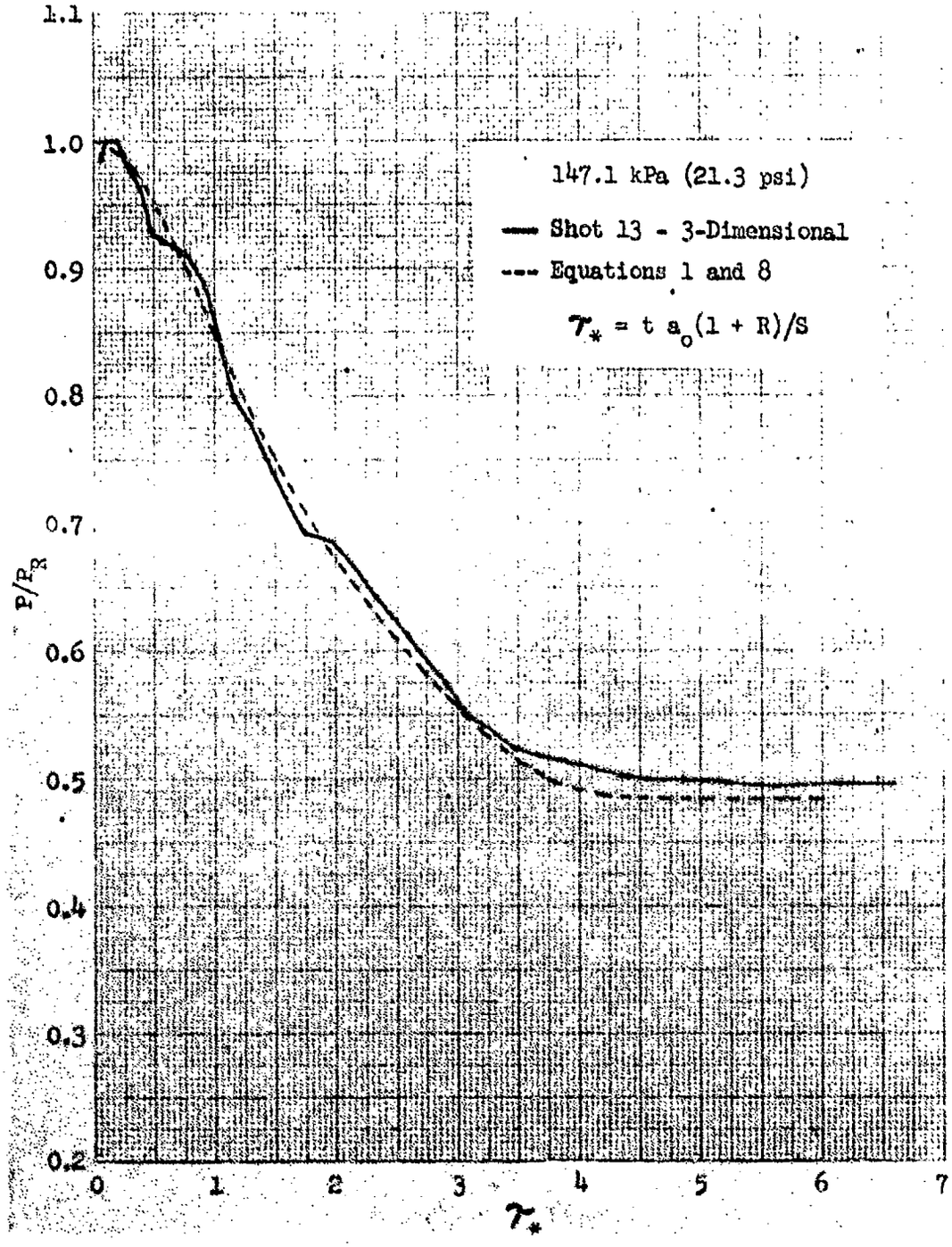

Figure 27 Average front surface pressure ratio of the three-dimensional shock tube target for an incident shock overpressure of 147.1 kPa (21.3 psi) plotted versus $\tau_* = t\, a_o(1 + R)/S$.

One requirement for use with the overturning code is that the prediction equation used should provide reasonable predictions over the range of incident shock overpressures from 13 to 345 kPa (2 to 50 psi). Figures 28 and 29 show predictions made using Equation 1 with functions as defined by Equation 4 and Equation 8 for a target with R = 0.5, S = 2 metres, P_A = 101.325 kPa (14.969 psi) and T_A = 15°C. It was assumed that no decay occurred behind the shock front. For both overpressure extremes the fit versus τ_* (Equation 8) is higher initially and lower later than the fit versus τ (Equation 4). No data were available to provide a basis for selecting one fit in preference to another. The fit provided by Equations 1 and 4 was selected as the preferred fit because the pressures predicted are lower at early times than the fit provided by Equations 1 and 8. Additional data are required to determine which of the two fits is best, and whether fitting against τ rather than against τ_* will provide the simplest representation over the widest range of incident shock overpressures.

III. REAR SURFACE LOADING

In Reference 2, Taylor presents average loading data for rear surfaces for the configurations shown in Figures 2C and 2D. Figures 30 and 31 show these data. The average pressure ratio for the rear surface is shown plotted versus τ_B, where $\tau_B = t\, a_o/S$. Note that this time normalization does not include the parameter R. The two-dimensional configuration (R = 0) is configuration D, and the three-dimensional configuration (R = 1) is configuration C. The curves were obtained by averaging the output of the three gages shown in Figure 1 according to the relation

$$P_{average} = (2A + C + D)/4$$

Although this relation was shown to provide a good average for the three-dimensional configuration at 34.47 kPa (5 psi) in Reference 5, the placement of gages and this averaging procedure seems less suitable for the two-dimensional configuration. However, there were no hydrocode data at hand to use to evaluate this averaging procedure for the two-dimensional configuration.

The curves from Reference 2 shown in Figures 30 and 31 do not indicate the initial time delay which corresponds to the time between shock arrival at the edge of the rear face when loading of the rear surface begins, and wave arrival at the gage nearest an edge. This time difference was not measured in the program of Reference 2. However, the initial wave crossing the rear surface must be a weak shock wave as shown by the low pressure at the initial rise of gage records. The velocity of this initial wave must be very near the sound velocity in undisturbed air, and hence this sound velocity was used to compute the initial delay for the average loading records. The time delays expressed in terms of τ_B were 0.488 for the two-dimensional configuration and 0.166 for the three-dimensional configuration.

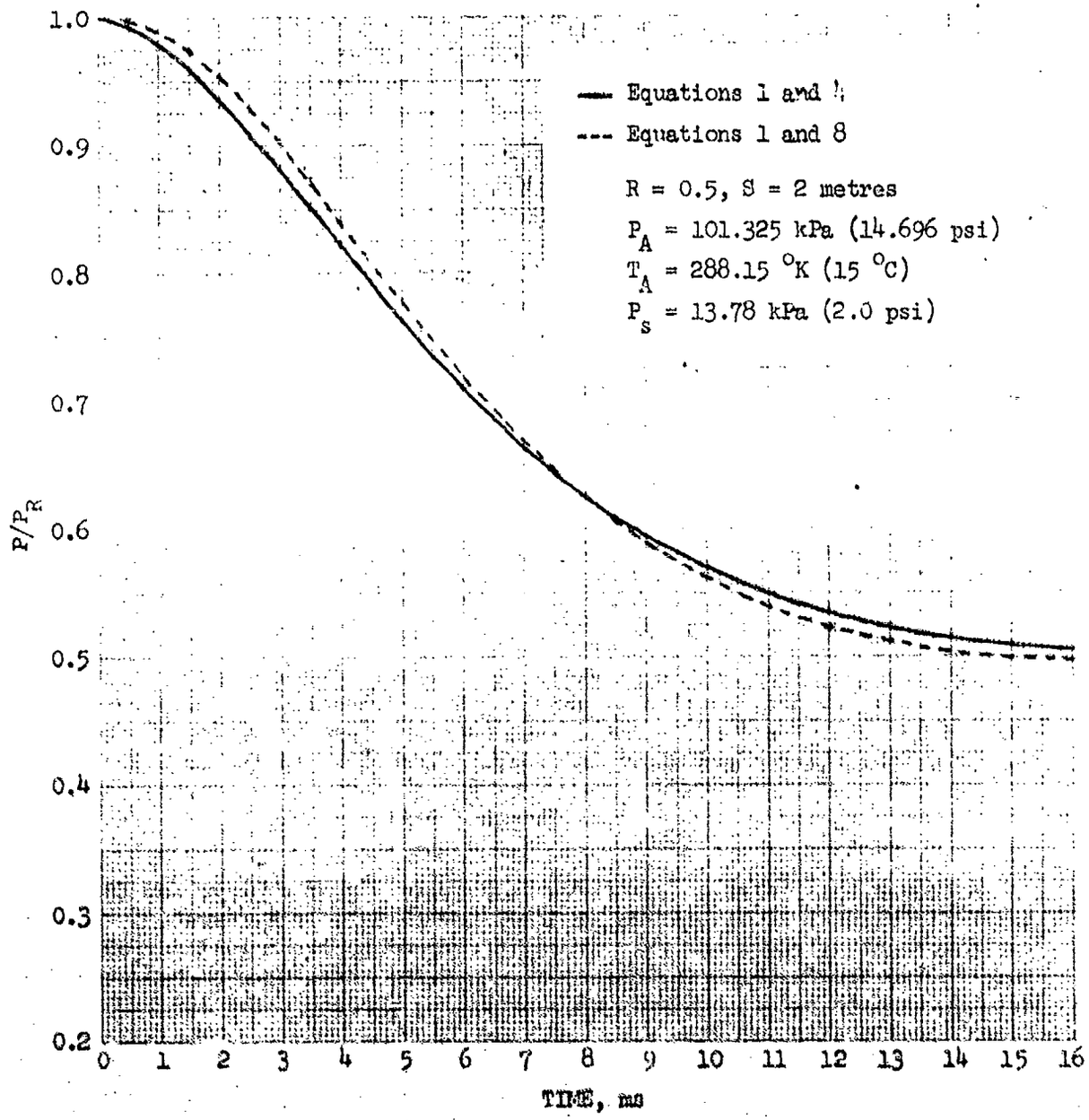

Figure 28 Predictions of front surface pressure ratios using Equations 1 and 4 and Equations 1 and 8 for an incident shock overpressure of 13.78 kPa (2.0 psi)

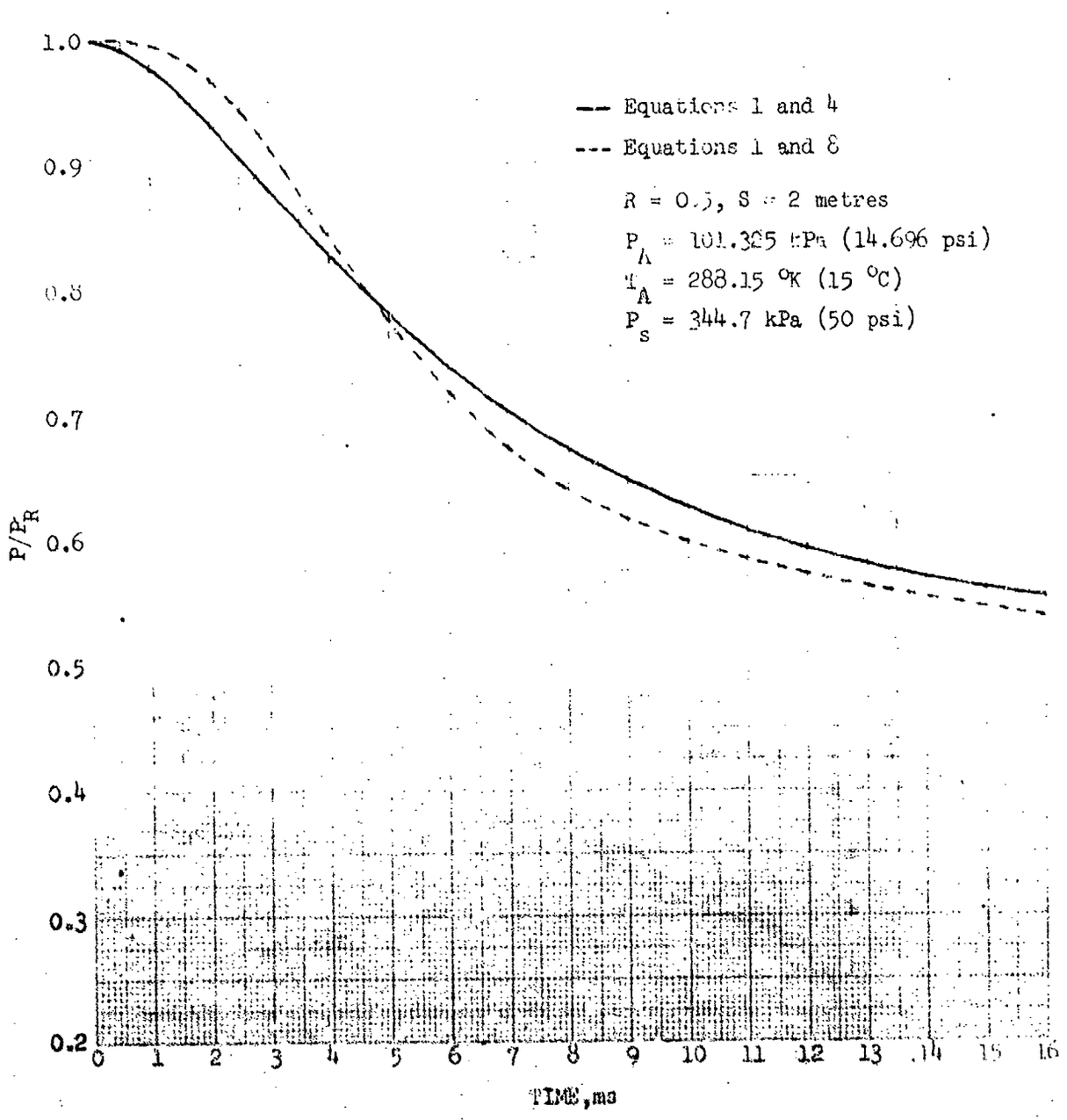

Figure 29 Predictions of front surface pressure ratios using Equations 1 and 4 and Equations 1 and 8 for an incident shock overpressure of 344.7 kPa (50 psi).

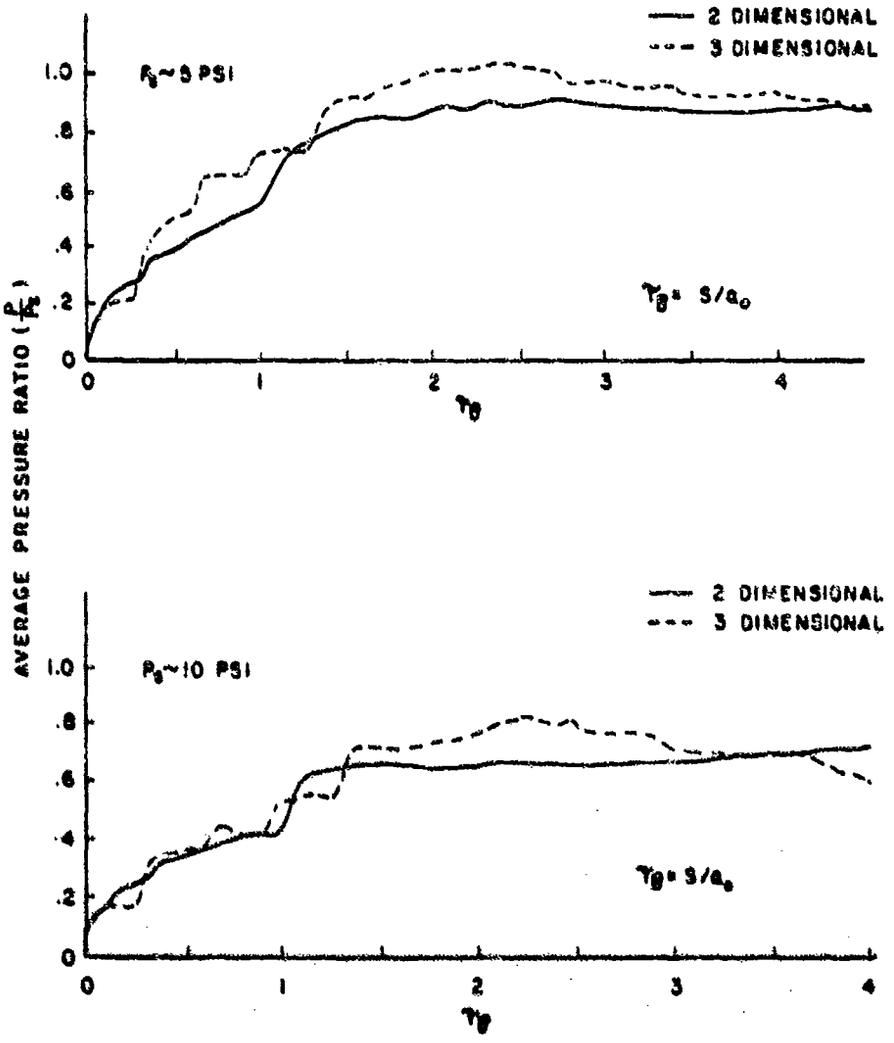

Figure 30 Average pressure ratios on rear surface of shock tube target for 34.5 and 68.9 kPa (5 and 10 psi) shock waves (from Reference 2).

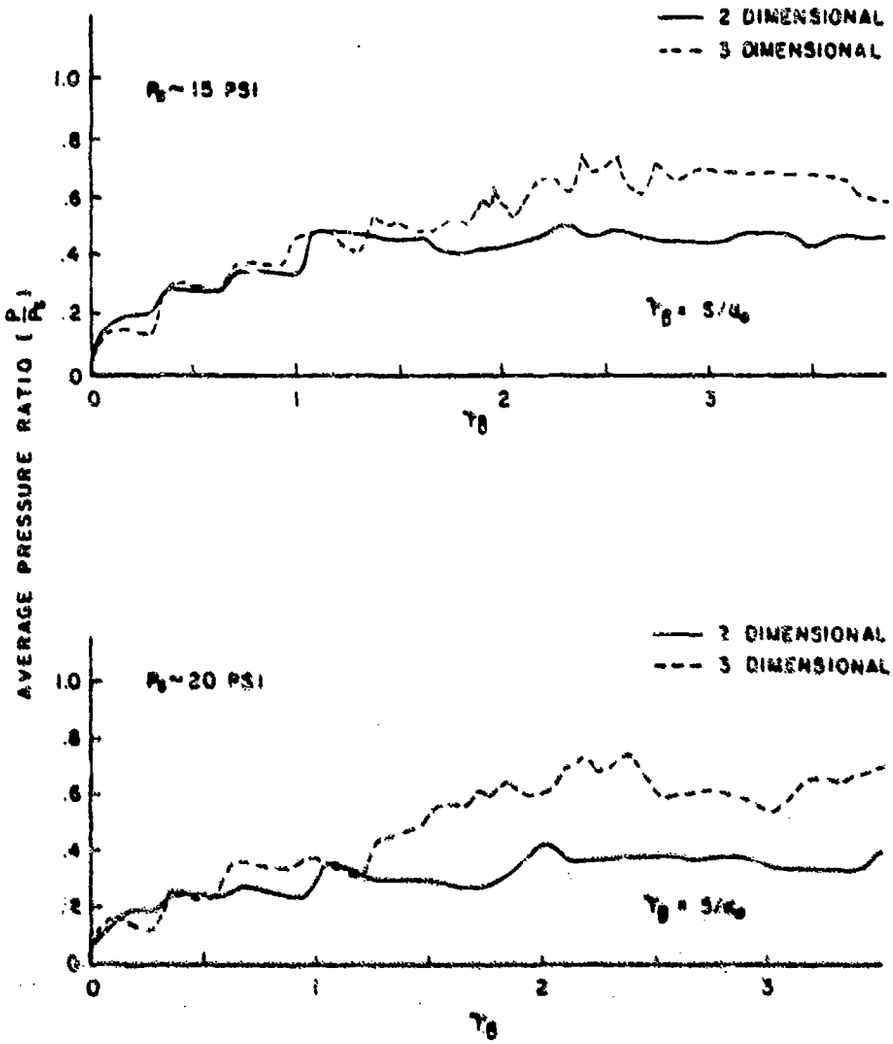

Figure 31 Average pressure ratios on rear surface of shock tube target for 103.4 and 137.9 kPa (15 and 20 psi) shock waves (from Reference 2).

Figures 32 and 33 show the curves from Figures 30 and 31 with the time delay for wave arrival included so that $\tau_B = 0$ corresponds to the initiation of loading on the rear surface. Values were estimated for the average maximum pressure ratio achieved on the rear surface at the conclusion of the initial rise of the record. These values are listed as P_{RM}/P_s in Table 1, where P_{RM} is the estimated maximum average pressure on the rear surface and P_s is the incident peak overpressure. This ratio is shown plotted versus $z = P_s/P_A$ in Figure 34.

A. Fitting an Equation for Average Rear Surface Pressure

The curves in Figures 32 and 33 for experimental data were normalized so that the ordinate value of 1.0 corresponds to the value of P_{RM}/P_s. It was found that the following relation provided what seems to be a good average curve for both the two and three-dimensional configurations:

$$\frac{P}{P_{RM}} = (1 - e^{-0.71\tau_B}(1 + 0.16\tau_B^2)) \qquad (9)$$

Figure 35 shows the normalized curves superimposed without regard for individual shot identification for the two and three-dimensional configurations. The dashed curve shown in each plot is the plot of Equation 9.

Figure 36 shows the normalized curves for the two-dimensional configuration for Shot 3 (32.82 kPa or 4.76 psi) and Shot 6 (139.4 kPa or 20.22 psi) and for Equation 9. Figure 37 shows a similar plot for Shot 2 (32.96 kPa or 4.78 psi) and Shot 10 (148.5 kPa or 21.54 psi) for the three-dimensional configuration. There is an indication of a variation in shape with z, the incident shock pressure ratio. In Figure 37 the curve for the lower pressure seems to rise faster than the curve for the higher pressure. The curves shown in Figure 36 also suggest a variation with z. In the initial part of the record the variation is the opposite of that shown in Figure 37, while for $\tau_B > 1.75$ the curve for the higher z does seem to be lower than that for the lower z.

Another study[6] shows a variation with incident overpressure level for a configuration corresponding to R = 1 or the three-dimensional configuration. Considering this fact, and that the more usual structure of interest more nearly corresponds to the three-dimensional rather than the two-dimensional configuration, an equation was fitted considering the z dependence as shown by the three-dimensional configuration. Because of the uncertainty in the accuracy of the average pressure for the two-dimensional configuration and the mixed variation with z shown, no attempt was made to fit a variation with z for the two-dimensional configuration. Instead, the same variation as found for the three-dimensional configuration was assumed to apply for both cases, and for all values of R between 0 and 1.

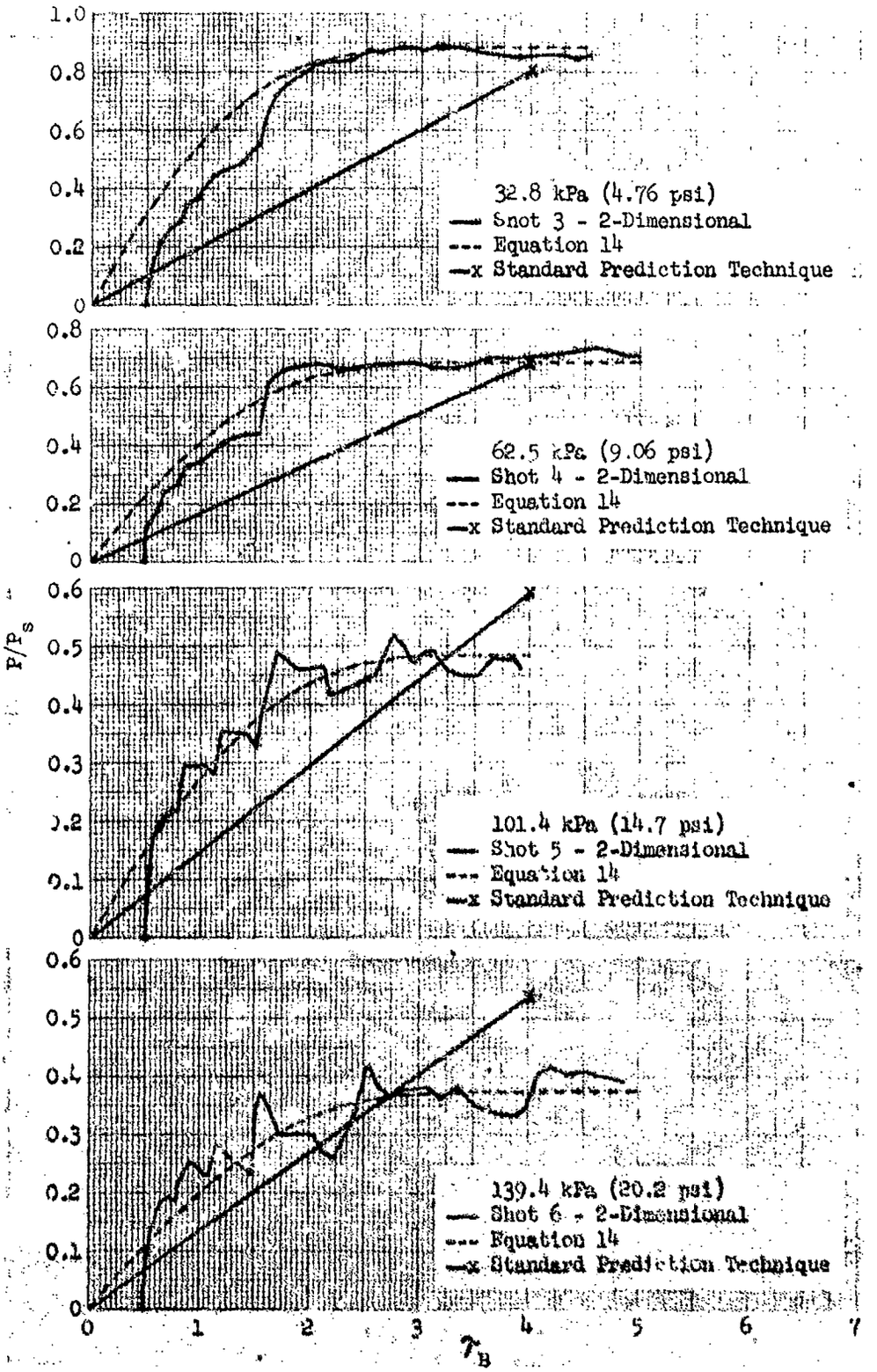

Figure 32 Average pressure ratios on the rear face of a two-dimensional shock tube target plotted versus $\tau_B = t\, a_o/S$, with delay for wave arrival included. Plots of a fitted equation and a standard prediction technique are shown.

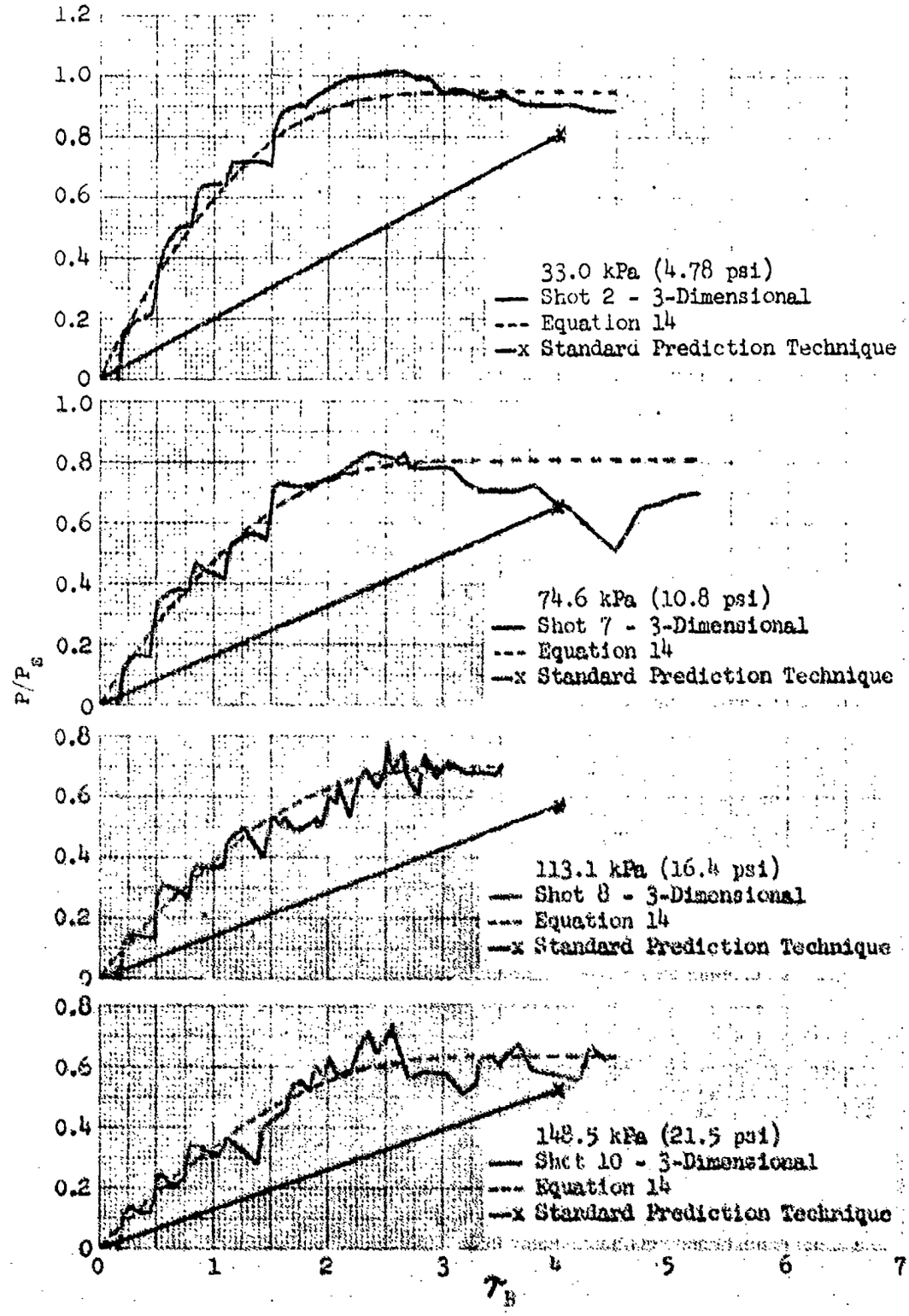

Figure 33 Average pressure ratios on the rear face of a three-dimensional shock tube target plotted versus $\tau_B = t\, a_o/\ell$, with delay for wave arrival included. Plots of a fitted equation and a standard prediction technique are shown.

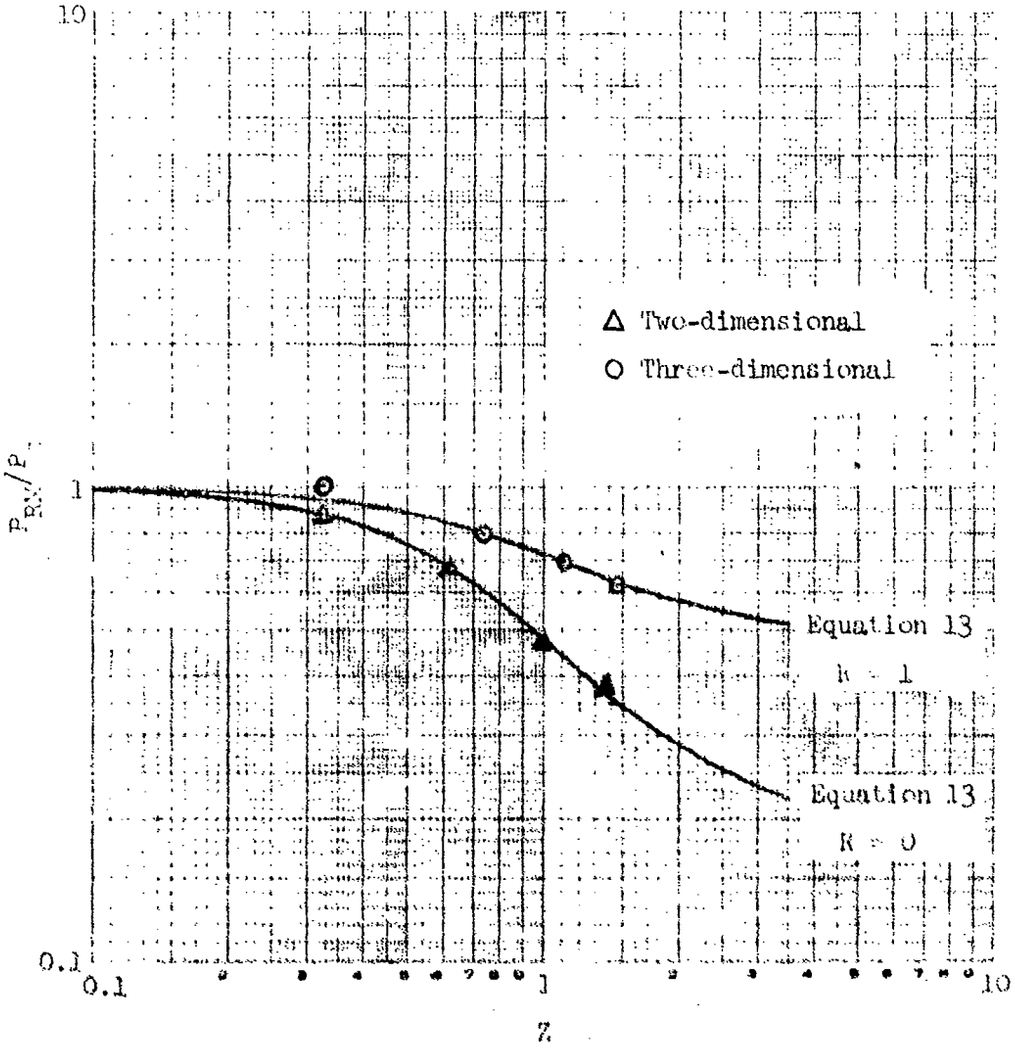

Figure 34 Average maximum pressure ratio on rear surface of shock tube target after initial pressure rise versus $z = P_s/P_A$. Plots of a fitted equation are shown.

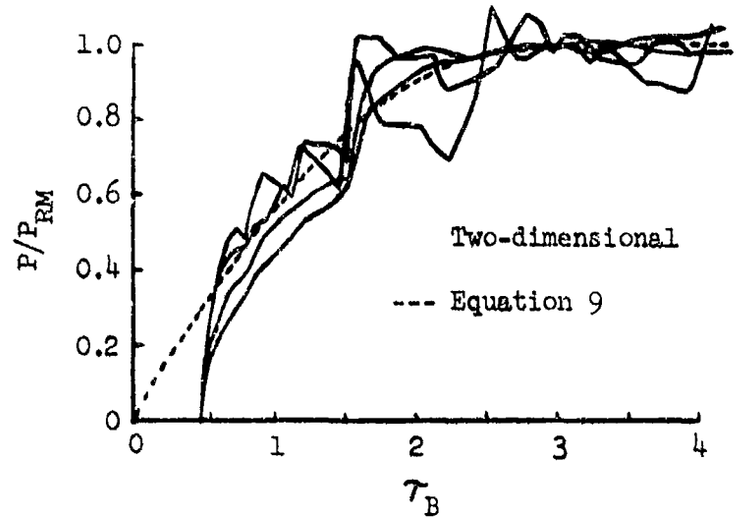

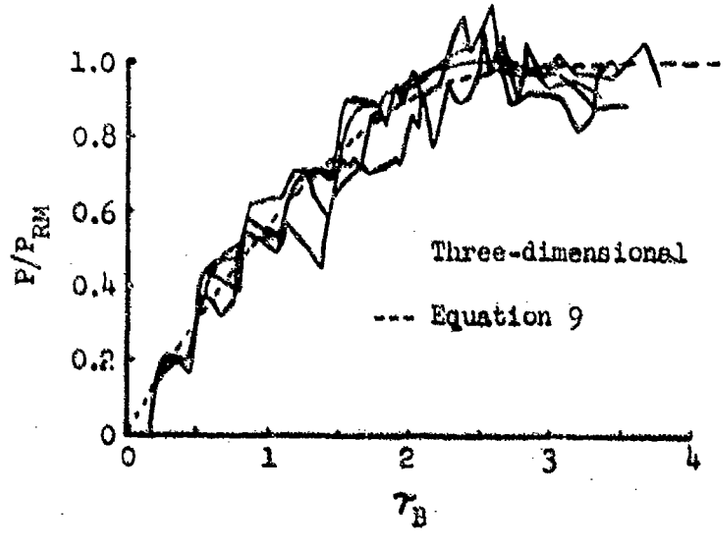

Figure 35 Pressure on the rear surface of shock tube target normalized to average maximum pressure after initial pressure rise versus $\tau_B = t\, a_o/S$. Plots of a fitted equation are shown.

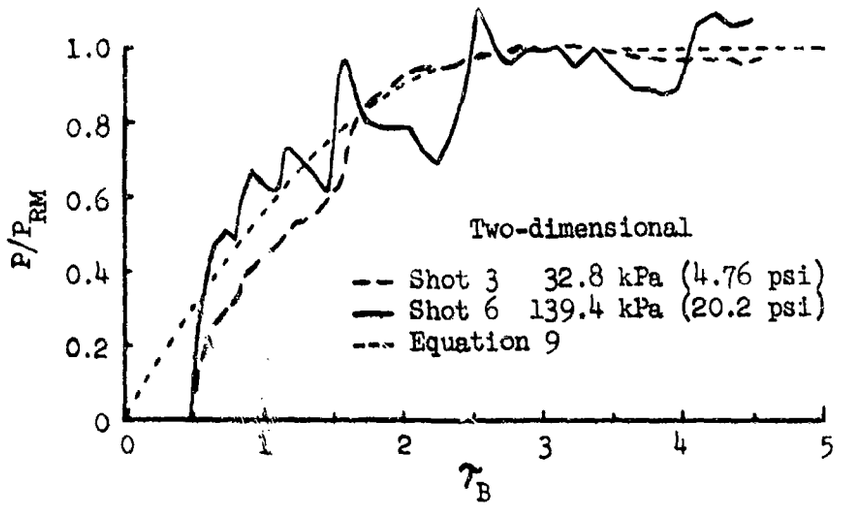

Figure 36 Comparison of pressure ratios on rear surface of a two-dimensional shock tube target for maximum and minimum incident shock overpressures used in an experimental study[2]. The plot of a fitted equation is shown.

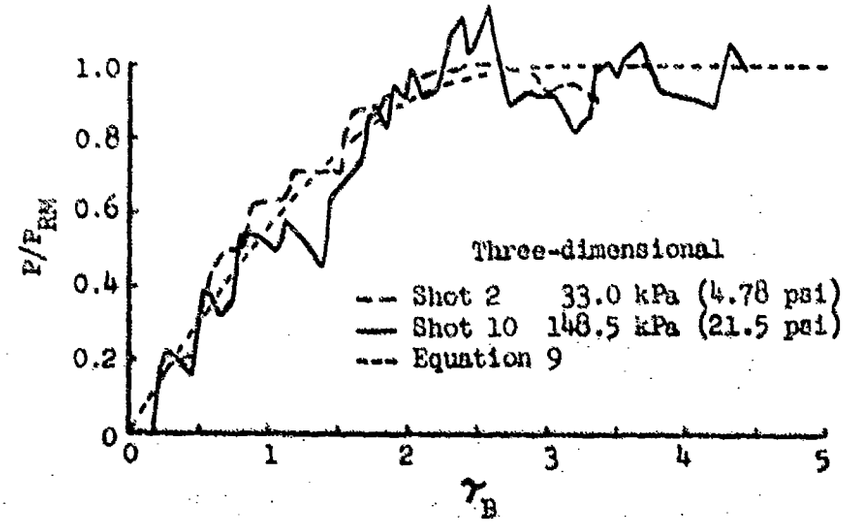

Figure 37 Comparison of pressure ratios on rear surface of a three-dimensional shock tube target for maximum and minimum incident shock overpressures used in an experimental study[2]. The plot of a fitted equation is shown.

The equation fitted was

$$\frac{P}{P_{RM}} = 1 - e^{-0.94e^{-0.27z}\tau_B(1 + 0.16\tau_B^2)} \qquad (10)$$

Figures 38 and 39 show the normalized records with the fit from Equation 10 plotted as the dashed curve.

To develop a complete prediction equation for the rear surface pressure, it was necessary to find equations for the maximum rear surface pressure used as normalizing factors. These data are shown in Figure 34. A difficulty added in the fitting process was the requirement for finding relations which would behave in a reasonable fashion when used outside the range of fitting, say over the range of z from 0.1 to 3.4. The relations found were as follows:

Two-dimensional, R = 0

$$\frac{P_{RM}}{P_s} = e^{-0.73z^{0.5}} + 1.4e^{-0.83z} \qquad (11)$$

Three-dimensional, R = 1

$$\frac{P_{RM}}{P_s} = e^{-0.32z^{0.5}} + 1.4e^{-0.83z} \qquad (12)$$

The equations where combined to predict values for the variation of R between 0 and 1 as follows:

$$\frac{P_{RM}}{P_s} = e^{-(0.73 - 0.41R)z^{0.5}} + 1.4e^{-0.83z} \qquad (13)$$

The curves shown in Figure 34 are plots of this equation with R = 0.

The final prediction equation for average pressure on the rear surface is the combination of Equations 10 and 13, and is as follows:

$$\frac{P}{P_s} = \left\{e^{-(0.73 - 0.41R)z^{0.5}} + 1.4e^{-0.83z}\right\}\left[1 - e^{-0.94e^{-0.27z}\tau_B(1 + 0.16\tau_B^2)}\right] \qquad (14)$$

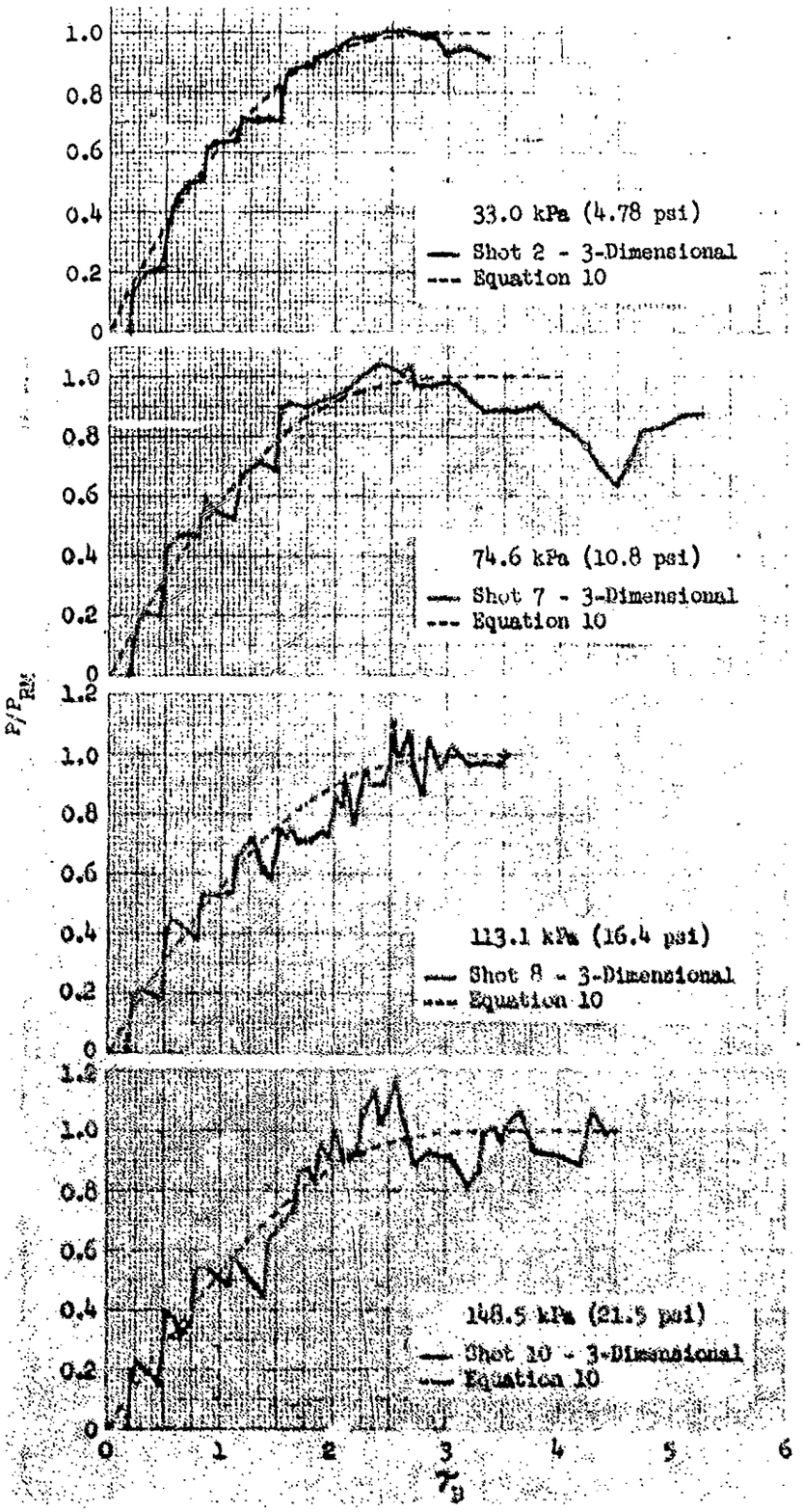

Figure 38 Average normalized pressure ratio on the rear surface of a three-dimensional shock tube target compared with a fitted equation.

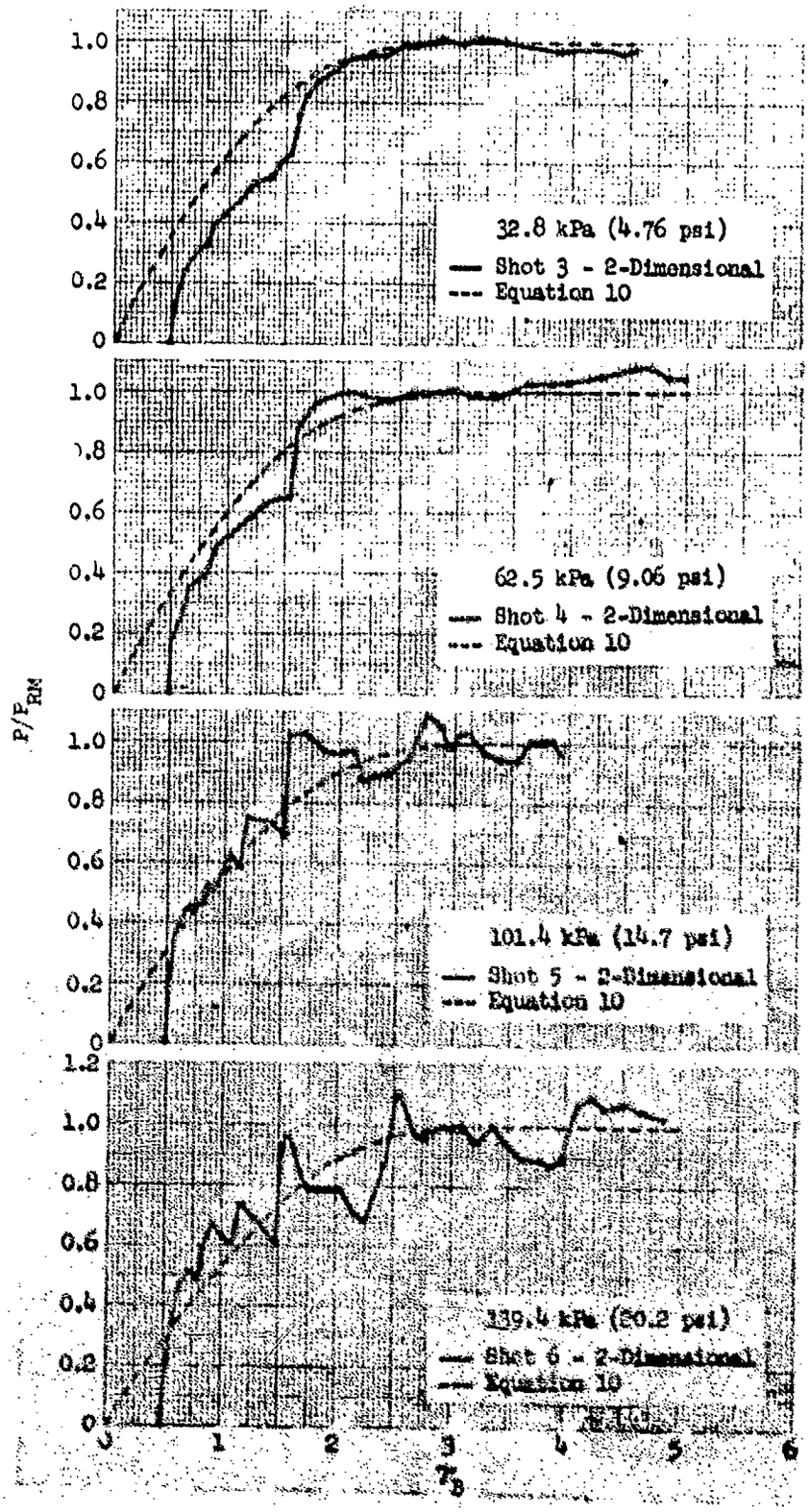

Figure 39 Average normalized pressure ratio on the rear surface of a two-dimensional shock tube target compared with a fitted equation.

The dashed curves in Figures 32 and 33 were calculated using this equation, and the quality of the fit can be judged from these plots. The fit is best for the three-dimensional configuration, where R = 1.

B. Comparison with Other Shock Tube Data

In Reference 6 rear surface average pressures are shown for a configuration for R = 1. Figure 40 shows these data compared with the predictions from Equation 14. The multiple curvatures shown by the experimental data are not modeled by the equation, but the equation does seem to provide a curve which fairs reasonably through the data.

C. Comparison with a Three-Dimensional Hydrocode Calculation

Figure 41 presents a comparison of the predicted curve calculated using Equation 14 with results from a hydrocode calculation for the average pressure on the rear surface of an S-280 Electrical Equipment Shelter[7]. The calculation was made for an incident shock front overpressure of 34.475 kPa (5 psi). It was assumed that no decay occurred behind the shock front. The calculation is reported in detail in Reference 7. The agreement shown in Figure 41 seems satisfactory.

D. Comparison with Standard Prediction Techniques

In Reference 3 the average pressure rise on the rear surface is approximated by a linear increase from the time of arrival of the shock front at the rear surface to a maximum value given by:

$$\frac{P_{RM}}{P_s} = \frac{1}{2}\left[1 + (1 - 0.5z)e^{-0.5z}\right] \qquad (15)$$

The time for the rise is specified as $t = 4S/a_o$, which corresponds to $\tau_B = 4$.

Predictions using this technique are shown as the straight lines in Figures 32 and 33, with the X indicating the maximum value. The large discrepancy emphasized by Taylor[2] between the straight-line approximation and the shock tube data is evident.

E. Modification to Account for Decay of the Incident Blast Wave

When the overpressure behind the incident shock front decreases with time as occurs in a blast wave, the average pressure on the rear surface is assumed to be reduced in proportion to the reduction in incident pressure from its peak value. Equation 14 remains unchanged except that $P_s(t)$ is substituted for P_s, the peak incident overpressure.

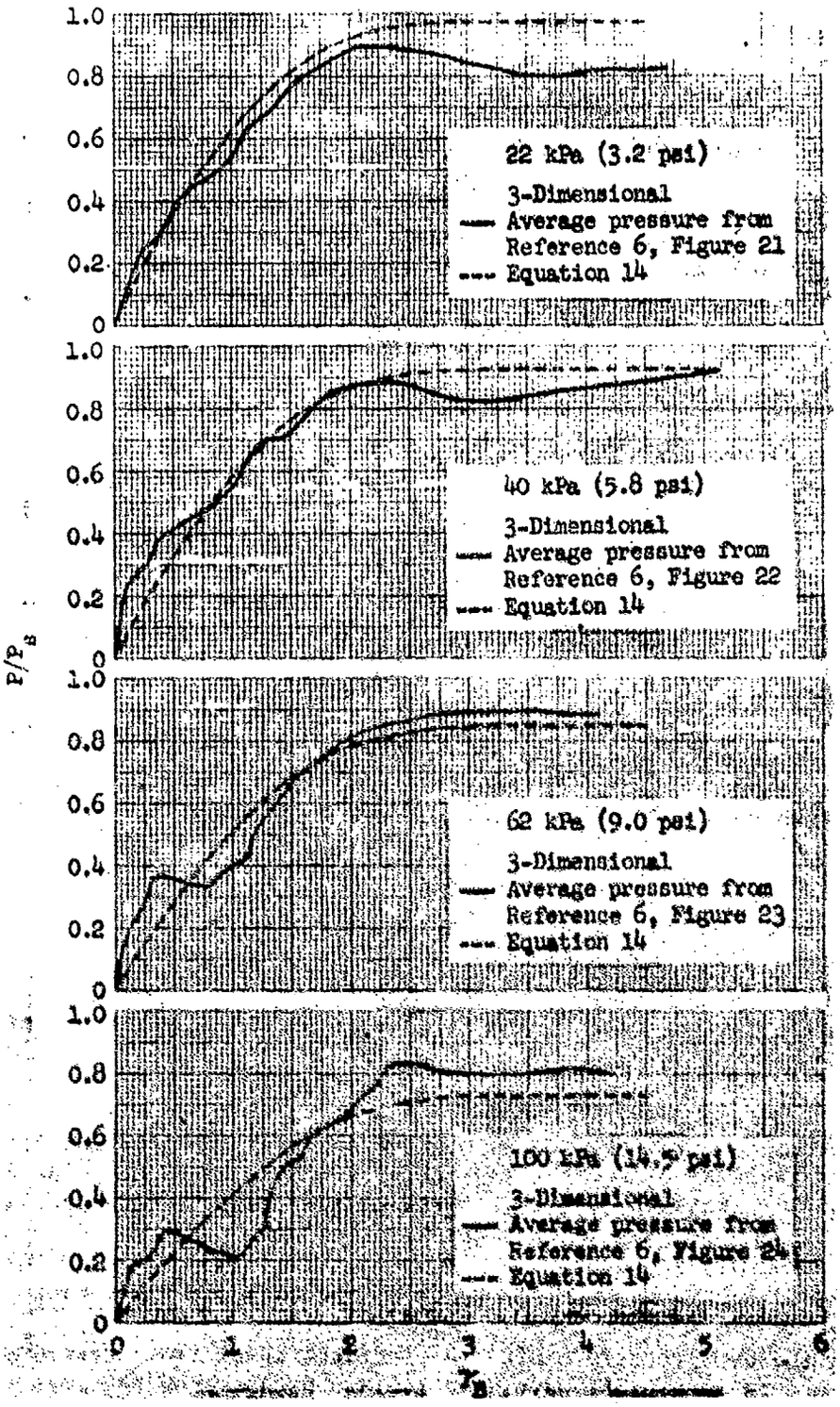

Figure 40 Comparison of rear surface pressure ratios for the three-dimensional shock tube target of Reference 6 with an equation fitted to the shock tube data of Reference 2.

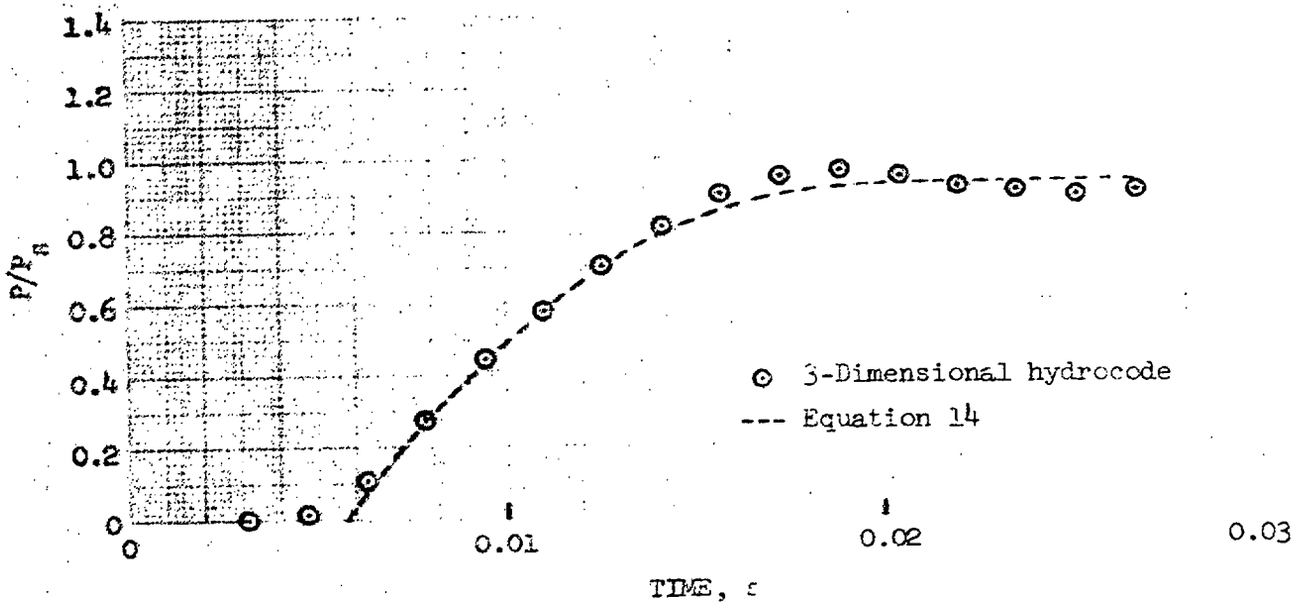

Figure 41 Comparison of average pressure ratio computed[7] for an S-280 Electrical Equipment Shelter using a three-dimensional hydrocode (BAAL) with Equation 14 for an incident shock overpressure of 34.47 kPa (5 psi).

F. Modification for Code Use

The suggested form of the average front surface pressure function for incorporation into the overturning code of Reference 1 decays to stagnation overpressure as shown in Equation 4. The particular overturning code terminates the calculation of diffraction loading when the overturning moment due to drag loading becomes equal to or exceeds that due to the diffraction moment. Assuming equal diffraction and drag loading areas and moment arms, the moments are equal at late times when:

$$P_{stag} - P_{rear} = C_d P_q$$

where: P_{stag} = peak stagnation overpressure

P_{rear} = ultimate average overpressure on rear surface

C_d = drag coefficient

P_q = peak dynamic pressure.

To insure that the diffraction loading calculation terminates in a reasonable time with an appropriate match between the diffraction and drag loading, the asymptotic value of P_{rear} was adjusted so that

$$P_{stag} - P_{rear} = 0.97\, C_d P_q.$$

The choice of the factor 0.97 is arbitrary, but its use is expected to produce a transition where the diffraction loading essentially has been completed. Then the value for P_{rear} is:

$$P_{rear} = P_{stag} - 0.97\, C_d P_q. \tag{16}$$

For a blast wave where the pressure decays with time, $P_{stag}(t)$ and $P_q(t)$ are substituted for P_{stag} and P_q, respectively. Then the prediction relation appropriate for incorporation into an overturning code is:

$$P(t) = (P_{stag}(t) - 0.97\, C_d P_q(t)) \left\{1 - e^{-0.94e^{-0.27z}\tau_B(1 + 0.16\tau_B^2)}\right\}. \tag{17}$$

IV. DISCUSSION

Equations for predicting average pressure on the front and rear surfaces of a rectangular parallelepiped have been developed by fairing

curves through a limited set of data from Reference 2. The equations fitted for the three-dimensional configuration provide reasonable agreement with shock tube data from References 2 and 6 in the overpressure range from 22 to 138 kPa (3 to 20 psi) and with a hydrocode calculation[7] at 34.475 kPa (5 psi). The validity of the fits for the two-dimensional configuration is subject to question because the placement and weighting of the gage records in Reference 2 does not seem as suitable for the two-dimensional configuration as for the three-dimensional configuration. Thus the equations fitted for the two-dimensional configuration should be regarded as an interim fit which may be improved if additional shock tube data and hydrocode calculations become available and are utilized. Because the two-dimensional results are incorporated in the final prediction equations where R varies between 0 and 1, the confidence in the prediction should decrease somewhat as R approaches zero.

It was found that the available shock tube data for average front surface overpressure could be fitted satisfactorily against either the dimensionless parameter $\tau = t\, a_5(1 + R)/S$ or $\tau_+ = t\, a_o\, (1 + R)/S$. Additional data for a wider range of shock overpressures are required to determine which of the two parameters can be used to obtain the most useful fit.

The prediction equations provide smooth extrapolations to the extreme values of overpressure of interest (13 to 345 kPa, or 2 to 50 psi), but the validity of the extrapolation at these extremes is not established. Additional data, particularly at overpressures above 20 psi, are required for values of R between 0 and 1 to provide a basis for properly accounting for the variation of predicted average pressure with R. The modifications to account for decay of pressure behind the incident shock front should be evaluated if appropriate data become available.

ACKNOWLEDGEMENTS

Appreciation is expressed to Mr. W. J. Taylor for providing data from his shock tube experiments and for many discussions concerning them, and to Mr. R. E. Lottero for tabulations of hydrocode results.

REFERENCES

1. N. H. Ethridge, "Blast Overturning Model for Ground Targets," BRL Report 1889, June 1976. (AD #B012102L)

2. W. J. Taylor, "A Method for Predicting Blast Loads During the Diffraction Phase," USA Ballistic Research Laboratories, Aberdeen Proving Ground, Maryland; included in Part 4, Bulletin 42, The Shock and Vibration Bulletin, The Shock and Vibration Information Center, Naval Research Laboratory, Washington, D. C., January 1972.

3. C. H. Norris, et al., "Structural Design for Dynamic Loads," McGraw-Hill Book Company, Inc., New York, N. Y., 1959.

4. W. J. Taylor, Private Communication.

5. R. A. Gentry, et al., "Three Dimensional Computer Analysis of Shock Loads on a Simple Structure," BRL CR 219, USA Ballistic Research Laboratories, Aberdeen Proving Ground, MD, March 1975. (AD #B003208L)

6. C. N. Kingery and J. H. Keefer, "Air Blast Loading on a Three-Dimensional Structure," BRL Report 952, AFSWP Report 813, July 1955. (AD #78562)

7. R. E. Lottero, "Computational Predictions of Shock Diffraction Loading on an S-280 Electrical Equipment Shelter," BRL Memorandum Report 2599, March 1976. (AD #A022804)

8. R. E. Shear and R. C. Makino, "A Non-Linear Shock Wave Reflection Theory," BRL Report 1351, January 1967 (AD 649945).

LIST OF SYMBOLS

Symbol

A = function of time, incident overpressure, ambient overpressure, and R used in equations fitted to average pressure profiles.

a = parameter used in a fitted equation.

a_o = ambient sound velocity = $331.32 \sqrt{\frac{T_A}{273.16}}$ m/s.

a_5 = velocity of the rarefaction wave behind the reflected shock wave = $a_o \sqrt{\frac{(8z + 7)(2z + 7)}{7(7 + 6z)}}$

B = function of time, incident overpressure, ambient overpressure, and R used in equations fitted to average pressure profiles.

C_d = drag coefficient for a blast target.

CONF = symbol meaning configuration

P = average overpressure on front surface or rear surface.

$P(t)$ = average overpressure versus time for a front or rear surface.

$P_{average}$ = average pressure on front surface.

P_A = ambient atmospheric pressure.

P_L = overpressure approached as a limit on the front surface.

P_q = peak dynamic pressure.

$P_q(t)$ = dynamic pressure versus time for a blast wave.

P_R = Peak reflected overpressure = $2 P_s (4z + 7)/(z + 7)$.

P_{rear} = average pressure on rear surface approached as a limit as time increases.

P_{RM} = estimated maximum average overpressure on rear surface after initial pressure rise.

Symbol

P_s = peak incident shock overpressure.

$P_s(t)$ = overpressure versus time for a blast wave.

P_{stag} = stagnation overpressure on the front surface; which for a non-decaying shock wave and a Mach number less than one is:

$$P_{stag} = (P_s + P_A)\left(1 + \frac{5z^2}{7(z+1)(z+7)}\right)^{7/2} - P_A$$

$P_{stag}(t)$ = stagnation overpressure at time t on front surface, which for Mach number less than one is:

$$P_{stag}(t) = (P_s(t) + P_A)\left[1 + (2/7)\frac{P_q(t)}{(P_s(t) + P_A)}\right]^{7/2} - P_A$$

R = ratio of the edges of the minimum rectangular area which must be examined to define loading over the entire surface area. The ratio is taken so that R ranges from 0 for the two-dimensional configuration to 1 for the three-dimensional configuration.

S = minimum distance of travel from an edge of a front or rear surface for a wave to traverse the surface.

t = time.

t_* = time for decay of front surface average overpressure in a standard prediction technique[3], $t_* = 3\ S/a_s$.

T_A = ambient atmospheric temperature, degrees Kelvin.

z = P_s/P_A, the ratio of peak incident shock overpressure to ambient atmospheric pressure.

α = parameter used in a fitted equation.

β = parameter used in a fitted equation.

γ = ratio of specific heats $\gamma = 1.4$ for an ideal gas.

τ = $t\ a_s(1 + R)/S$.

LIST OF SYMBOLS (Continued)

Symbol

τ_* = $t\, a_o(1 + R)/S$.

τ_B = $t\, a_o/S$.

2DF = symbol meaning two-dimensional configuration, front surface record.

2DR = symbol meaning two-dimensional configuration, rear surface record.

3DF = symbol meaning three-dimensional configuration, front surface record.

3DR = symbol meaning three-dimensional configuration, rear surface record.

DISTRIBUTION LIST

No. of Copies	Organization
12	Commander Defense Documentation Center ATTN: DDC-TCA Cameron Station Alexandria, VA 22314
5	Director Defense Advanced Research Projects Agency ATTN: Tech Lib NMRO PMO TTO TAO 1400 Wilson Boulevard Arlington, VA 22209
5	Director of Defense Research and Engineering ATTN: DDRCE DD/TWP DD/S&SS DD/I&SS AD/SW Washington, DC 20301
1	Director Weapons Systems Evaluation Gp ATTN: Document Control Washington, DC 20305
1	Director Institute for Defense Analyses ATTN: IDA Librarian, Ruth S. Smith 400 Army-Navy Drive Arlington, VA 22202
4	Asst. to the Secretary of Defense (Atomic Energy) ATTN: Nuc Policy Planning Strategic & Assesment Document Control Donald R. Cotter Washington, DC 20301
8	Director Defense Intelligence Agency ATTN: RDS-3C DN Dir-4 DT-1C DT-7D/E. O. Farrell DT-2/Wpns & Sys Div Technical Library DI-7E Washington, DC 20301
6	Director Defense Nuclear Agency ATTN: SPTD STSI/Archives SPAS/Mr. J. Moulton STSP STVL/Dr. La Vier RATN/Cdr Alderson Washington, DC 20305
13	Director Defense Nuclear Agency ATTN: DIR DDOA STNA STRA VLIS PORA VLWS/MAJ Chrobak DDST/Mr. P. Haas DDST/Mr. M. Atkins STTL/Tech Lib (2 cys) SPSS (2 cys) Washington, DC 20305

DISTRIBUTION LIST

No. of Copies	Organization
2	Commander Field Command, DNA ATTN: FCPR FCTMOF Kirtland AFB, NM 87115
1	Chief Las Vegas Liaison Office Field Command TD, DNA ATTN: Document Control P. O. Box 2702 Las Vegas, NV 89104
1	Commander Field Command, DNA Livermore Branch ATTN: FCPRL, L-395 P. O. Box 808 Livermore, CA 94550
1	Director Defense Communications Agency ATTN: Code B210, Wpn Sys Analysis Division Washington, DC 20305
4	Director Joint Strategic Target Planning Staff JCS ATTN: JSTPS/JPS JSTPS/JLTW JSTPS/JL JSTPS/JP Offutt AFB Omaha, NB 68113
2	Director National Security Agency ATTN: E. F. Butala, R15 F. Newton Ft. George G. Meade, MD 20755
1	Commander US Army Materiel Development and Readiness Command ATTN: DRCDMA-ST 5001 Eisenhower Avenue Alexandria, VA 22333
1	Commander US Army Materiel Development and Readiness Command ATTN: Technical Library 5001 Eisenhower Avenue Alexandria, VA 22333
1	Commander US Army Materiel Development and Readiness Command ATTN: DRCDR-D 5001 Eisenhower Avenue Alexandria, VA 22333
1	Commander US Army Materiel Development and Readiness Command ATTN: W. H. Hubbard 5001 Eisenhower Avenue Alexandria, VA 22333
1	Commandant National War College ATTN: NWCLB-CR Fort Lesley J. McNair Washington, DC 20315
1	Commander US Army Aviation Research and Development Command ATTN: DRSAV-E 12th and Spruce Streets St. Louis, MO 63166

DISTRIBUTION LIST

No. of Copies	Organization
1	Director US Army Air Mobility Research and Development Laboratory Ames Research Center Moffett Field, CA 94035
4	Commander US Army Electronics Command ATTN: DRSEL-RD DRSEL-TL-IR R. Freiberg A. Sigismondi E. T. Hunter Fort Monmouth, NJ 07703
3	Commander US Army Missile Materiel Readiness Command ATTN: DRSMI-R DRSMI-XS, Chief Scientist Technical Library Redstone Arsenal, AL 35809
3	Commander US Army Missile Research and Development Command ATTN: DRDMI-R DRDMI-XS, Chief Scientist Technical Library Redstone Arsenal, AL 35809
1	Commander US Army Tank Automotive Development Command ATTN: DRDTA-RWL Warren, MI 48090
2	Commander US Army Mobility Equipment Research and Development Command ATTN: Tech Docu Cen, Bldg. 315 DRSME-RZT Fort Belvoir, VA 22060
1	Commander US Army Armament Research and Development Command ATTN: Technical Library Rock Island, IL 61202
1	Commander US Army Armament Materiel Readiness Command ATTN: Technical Library Rock Island, IL 61202
3	Commander US Army Armament Research and Development Command ATTN: SARPA-ND-C P. Angelotti (2 cys) Technical Library Dover, NJ 07801
1	Commander US Army Watervliet Arsenal Watervliet, NY 12189

DISTRIBUTION LIST

No. of Copies	Organization
4	Commander US Army Harry Diamond Labs ATTN: Mr. James Gaul Mr. L. Belliveau Mr. J. Gwaltney Mr. F. N. Wimenitz Mr. W. Vault 2800 Powder Mill Road Adelphi, MD 20783
4	Commander US Army Harry Diamond Labs ATTN: DRXDO-RBA DRXDO-TI DRXDO-NP DRXDO-RBH Mr. P. A. Caldwell 2800 Powder Mill Road Adelphi, MD 20783
1	Commander US Army Materials and Mechanics Research Center ATTN: Technical Library Watertown, MA 02172
2	Commander US Army Natick Research and Development Command ATTN: DRXRE/Dr. D. Sieling DRXNM-UE Arthur Johnson Natick, MA 01762
1	Commander US Army Foreign Science and Technology Center ATTN: Rsch & Concepts Branch 220 7th Street, NE Charlottesville, VA 22901
2	Commander US Army Nuclear Agency ATTN: MONA-WE Tech Library 7500 Backlick Road, Bldg 2073 Springfield, VA 22150
2	Director US Army TRADOC Systems Analysis Activity ATTN: ATAA-SA ATAA-TAC White Sands Missile Range NM 88002
1	Commander US Army Electronics Proving Ground ATTN: STEEP-PA-I Fort Huachuca, AZ 85613
1	Commandant US Army Armor School ATTN: ATSB-CTD Fort Knox, KY 40121
1	Commander US Army Combined Arms Combat Development Activity ATTN: ATCA-CFT Ft. Leavenworth, KS 66027
1	Commandant US Army Comd and General Staff College Ft. Leavenworth, KS 66027
1	Commander US Army Concepts Analysis Agency ATTN: MOCA-WGP 8120 Woodmont Avenue Bethesda, MD 20014

DISTRIBUTION LIST

No. of Copies	Organization
1	Commander US Army Artillery School ATTN: ATSF-CTD Ft. Sill, OK 73503
1	Commandant US Army War College ATTN: Library Carlisle Barracks, PA 17013
1	Interservice Nuclear Weapons School ATTN: Technical Library Kirtland AFB, NM 87115
2	HQDA (DAMA-AR; NCL Div) Washington, DC 20310
2	Office, Chief of Engineers Department of the Army ATTN: DAEN-MCE-D DAEN-RDM 890 South Pickett Street Alexandria, VA 22304
2	Deputy Chief of Staff for Operations and Plans ATTN: Technical Library Director of Chemical and Nuclear Operations, Department of the Army Washington, DC 20310
2	Director US Army BMD Advanced Technology Center ATTN: CRDABH-X CRDABH-S Huntsville, AL 35807
1	Commander US Army Research Office P.O. Box 12211 Research Triangle Park NC 27709
5	Commander US Army Engineer Waterways Experiment Station ATTN: Technical Library William Flathau John N. Strange Guy Jackson Leo Ingram P. O. Box 631 Vicksburg, MS 39180
2	Director Defense Civil Preparedness Agency ATTN: Mr. George Sisson/RF-SR Technical Library Washington, DC 20301
1	Commander US Army Engineering Center ATTN: ATSEN-SY-L Fort Belvoir, VA 22060
1	Division Engineer US Army Engineering Division Ohio River ATTN: Docu Cen P. O. Box 1159 Cincinnati, OH 45201
1	Division Engineer US Army Engineering Division ATTN: HNDSE-R/M. M. Dembo Huntsville Box 1600 Huntsville, AL 35804

DISTRIBUTION LIST

No. of Copies	Organization
5	Chief of Naval Research ATTN: Code 464/Jacob L. Warner Code 464/Thomas P. Quinn Code 713 N. Perrone Technical Library Department of the Navy Washington, DC 20360
2	Chief of Naval Operations ATTN: OP-03EG OP-985F Department of the Navy Washington, DC 20350
1	Chief of Naval Material ATTN: MAT 0323 Department of the Navy Arlington, VA 22217
3	Director Strategic Systems Projects Ofc ATTN: NSP-43, Tech Lib NSP-273 NSP-272 Department of the Navy Washington, DC 20360
1	Commander Naval Electronic Systems Com ATTN: PME 117-21A Washington, DC 20360
2	Commander Naval Sea Systems Command ATTN: ORD-91313 Library Code 03511 Department of the Navy Washington, DC 20362
3	Commander US Naval Facilities Engineering Command ATTN: Code 03A Code 04B Technical Library Washington, DC 20360
3	Officer-in-Charge Civil Engineering Laboratory Naval Constr Btn Ctr ATTN: Stan Takahaski R. J. Odello Technical Library Port Hueneme, CA 93041
2	Commander Naval Ship Engineering Center ATTN: Technical Library NSEC 6105G Hyattsville, MD 20782
1	Commander David W. Taylor Naval Ship Research & Development Center ATTN: L42-3 Library Bethesda, MD 20084
3	Commander US Naval Surface Weapons Center ATTN: Code WA501/Navy Nuclear Programs Office Code WX21/Tech Lib Code 240/C. J. Aronson Silver Spring, MD 20910
1	Commander US Naval Surface Weapons Center ATTN: DX-21, Library Br Dahlgren, VA 22448

DISTRIBUTION LIST

No. of Copies	Organization
2	Commander US Naval Ship Research and Development Center Facility Underwater Explosions Research Division ATTN: Code 17/W. W. Murray Technical Library Portsmouth, VA 23709
1	Commander US Naval Weapons Center ATTN: Code 533/Tech Lib China Lake, CA 93555
2	Commander US Naval Weapons Evaluation Facility ATTN: Document Control R. Hughes Kirtland AFB Albuquerque, NM 87117
1	Commander US Naval Civil Engineering Laboratory ATTN: John Crawford Port Hueneme, CA 93041
2	Commander US Naval Research Laboratory ATTN: Code 2027/Tech Lib Code 8440/F. Rosenthal Washington, DC 20375
1	Superintendent US Naval Postgraduate School ATTN: Code 2124/Tech Rpts Lib Monterey, CA 93940
2	Commandant of the Marine Corps Navy Department ATTN: DCS(P&O) Req Div DCS(P&O) Strat Plans Div, Code PL Washington, DC 20380
1	Commanding General MCDEC ATTN: Commanding General Quantico, VA 22134
1	Superintendent Naval Academy ATTN: Classified Library Annapolis, MD 21402
1	President Naval War College ATTN: Tech Library Newport, RI 02840
1	HQ USAF (IN) Washington, DC 20330
1	HQ USAF (PRE) Washington, DC 20330
1	AFSC (Tech Lib) Andrews AFB Washington, DC 20331
2	AFATL (ATRD/R. Brandt) Eglin AFB, FL 32542
1	ADTC (Tech Lib) Eglin AFB, FL 32542
1	RADC (EMTLD/Docu Lib) Griffiss AFB, NY 13340
4	AFWL (SUL: DE-1; DEX; R. Henny) Kirtland AFB, NM 87117
4	AFWL (Robert Port; NSB DEV Jimmie L. Bratton; DEV M. A. Plamondon) Kirtland AFB, NM 87117

DISTRIBUTION LIST

No. of Copies	Organization
2	Commander-in-Chief Strategic Air Command ATTN: NRI-STINFO Lib XPFS Offut AFB, NB 68113
1	Commandant Air Command and Staff College ATTN: Library Maxwell Air Force Base, AL 36112
1	USAF School of Aerospace, AFSC ATTN: RA Chief Radiobiology Div Brooks Air Force Base, TX 78235
1	AFML (MAMD/Dr. T. Nicholas) Wright-Patterson AFB OH 45433
1	FTD (TD-BTA/Lib) Wright-Patterson AFB OH 45433
1	ASD (Tech Lib) Wright-Patterson AFB OH 45433
2	ADC (XP; XPQDQ) Wright-Patterson AFB OH 45433
1	AFIT (Lib Bldg.640,Area B) Wright-Patterson AFB OH 45433
1	Director US Bureau of Mines ATTN: Technical Library Denver Federal Center Denver, CO 80225
1	Director US Bureau of Mines Twin Cities Research Center ATTN: Technical Library P. O. Box 1660 Minneapolis, MN 55111
1	US Energy Research and Development Administration Division of Headquarters Svcs ATTN: Doc Control for Classified Tech Lib Library Branch G-043 Washington, DC 20545
1	US Energy Research and Development Administration Albuquerque Operations Office ATTN: Doc Control for Tech Lib P. O. Box 5400 Albuquerque, NM 87115
1	US Energy Research and Development Administration Nevada Operations Office ATTN: Doc Control for Tech Lib P. O. Box 14100 Las Vegas, NV 89114
5	Director Lawrence Livermore Laboratory ATTN: L. W. Woodruff/L-96 Tech Info Dept L-3 D. M. Norris/L-90 Ted Butkovich/L-200 J. R. Hearst/L-205 P. O. Box 808 Livermore, CA 94550
2	Sandia Laboratories ATTN: Doc Con for 3141 Sandia Report Coll. SSD 1315 P. O. Box 5800 Albuquerque, NM 87115
4	Director Lawrence Livermore Laboratory ATTN: Jack Kahn/L-7 J. Carothers/L-7 Robert Schock/L-437 R. G. Dong/L-90 P. O. Box 808 Livermore, CA 94550

DISTRIBUTION LIST

No. of Copies	Organization
2	Director Los Alamos Scientific Laboratory ATTN: Doc Control for Rpts Lib R. A. Gentry P. O. Box 1663 Los Alamos, NM 87544
1	Director National Aeronautics and Space Administration Scientific and Technical Information Facility P. O. Box 8757 Baltimore/Washington International Airport, MD 21240
2	Aerospace Corporation ATTN: Tech Info Services P. N. Mathur P. O. Box 92957 Los Angeles, CA 90009
1	Agbabian Associates ATTN: M. Agbabian 250 North Nash Street El Segundo, CA 90245
1	Analytic Services, Inc. ATTN: George Hesselbacher 5613 Leesburg Pike Falls Church, VA 22041
1	Applied Theory, Inc. ATTN: John G. Trulio 1010 Westwood Blvd. Los Angeles, CA 90024
1	Artec Associates, Inc. ATTN: Steven Gill 26046 Eden Landing Road Hayward, CA 94545
1	AVCO ATTN: Res Lib A830, Rm 7201 201 Lowell Street Wilmington, MA 01887
2	The BDM Corporation ATTN: Technical Library A. Lavagnino 1920 Aline Avenue Vienna, VA 22180
1	The BDM Corporation ATTN: Richard Hensley P. O. Box 9274 Albuquerque International Albuquerque, NM 87119
2	The Boeing Company ATTN: Aerospace Library R. H. Carlson P. O. Box 3707 Seattle, WA 98124
1	Brown Engineering Co., Inc. ATTN: Manu Patel Cummings Research Park Huntsville, AL 35807
2	California Research and Technology, Inc. ATTN: Ken Kreyenhagen Technical Library 6269 Variel Avenue Woodland Hills, CA 91364
1	Calspan Corporation ATTN: Technical Library P. O. Box 235 Buffalo, NY 14221

DISTRIBUTION LIST

No. of Copies	Organization
1	Civil/Nuclear Systems Corporation ATTN: Robert Crawford 1200 University N. E. Albuquerque, NM 87102
1	EG&G, Incorporated Albuquerque Division ATTN: Technical Library P. O. Box 10218 Albuquerque, NM 87114
1	The Franklin Institute ATTN: Zemons Zudans 20th Street and Parkway Philadelphia, PA 19103
1	General American Trans Corporation General American Research Division ATTN: G. L. Neidhardt 7449 N. Natchez Avenue Niles, IL 60648
1	General Electric Company-TEMPO ATTN: DASIAC P. O. Drawer QQ Santa Brabara, CA 93102
1	General Research Corporation ATTN: Benjamin Alexander P. O. Box 3587 Santa Barbarba, CA 93105
1	General Research Corporation Washington Operations ATTN: TAC Warfare Opns Westgate Research Park 7655 Old Springhouse Road, Suite 700 McLean, VA 22101
1	J. H. Wiggins Co., Inc. ATTN: John Collins 1650 South Pacific Coast Highway Redondo Beach, CA 90277
3	Kaman Avidyne ATTN: Dr. N. P. Hobbs Mr. S. Criscione Mr. John Calligeros 83 Second Avenue Northwest Industrial Park Burlington, MA 01830
3	Kaman Sciences Corporation ATTN: Library P. Sachs F. H. Shelton 1500 Garden of the Gods Road Colorado Springs, CO 80907
1	Lockheed Missiles & Space Co. ATTN: Technical Library P. O. Box 504 Sunnyvale, CA 94088
2	Martin Marietta Aerospace Orlando Division ATTN: G. Fotieo F. Marion P. O. Box 5837 Orlando, FL 32805
1	Mathematical Applications Group, Inc ATTN: M. O. Cohen 3 Westchester Plaza Elmsford, NY 10523
1	McDonnell Douglas Corporation ATTN: Robert W. Halprin 5301 Bolsa Avenue Huntington Beach, CA 92647

DISTRIBUTION LIST

No. of Copies	Organization
2	Merritt Cases, Inc. ATTN: J. L. Merritt Technical Library P. O. Box 1206 Redlands, CA 92373
1	Meteorology Research, Inc. ATTN: W. D. Green 464 West Woodbury Road Altadena, CA 91001
1	The Mitre Corporation ATTN: Library P. O. Box 208 Bedford, MA 01730
1	Pacific Sierra Research Corporation ATTN: Gary Lang 1456 Cloverfield Boulevard Santa Monica, CA 90404
2	Pacifica Technology ATTN: G. Kent R. Bjork P. O. Box 148 Del Mar, CA 92014
2	Physics International Corp. ATTN: E. T. Moore F. N. Sauer 2700 Merced Street San Leandro, CA 94577
3	Physics International Corp ATTN: Charles Godfrey Larry A. Behrmann Technical Library 2700 Merced Street San Leandro, CA 94577
5	R&D Associates ATTN: Dr. H. L. Brode Dr. Albert L. Latter C. P. Knowles William B. Wright Henry Cooper P. O. Box 9695 Marina del Rey, CA 90291
4	R&D Associates ATTN: Jerry Carpenter Sheldon Schuster J. G. Lewis Technical Library P. O. Box 9695 Marina del Rey, CA 90291
1	R&D Associates ATTN: J. Thompson 1815 N. Ft. Meyer Drive 11th Floor Arlington, VA 22209
1	The Rand Corporation ATTN: C. C. Mow 1700 Main Street Santa Monica, CA 90406
6	Sandia Laboratories ATTN: Doc Control for 3141 Sandia Rpt Collection A. J. Chaban N. L. Norritt L. J. Vortman W. Roherty L. Hill Albuquerque, NM 87115

DISTRIBUTION LIST

No. of Copies	Organization
1	Sandia Laboratories Livermore Laboratory ATTN: Doc Control for Tech Lib P. O. Box 969 Livermore, CA 94550
1	Science Applications, Inc. ATTN: Technical Library P. O. Box 3507 Albuquerque, NM 87110
2	Science Applications, Inc ATTN: R. Seebaugh John Mansfield 1651 Old Meadow Road McLean, VA 22101
1	Science Applications, Inc. 8201 Capwell Drive Oakland, CA 94621
2	Science Applications, Inc. ATTN: Technical Library Michael McKay P. O. Box 2351 La Jolla, CA 92038
2	Systems, Science & Software ATTN: Donald R. Grine Technical Library P. O. Box 1620 La Jolla, CA 92037
1	Terra Tek, Inc. ATTN: Technical Library 420 Wakara Way Salt Lake City, UT 84108
1	Tetra Tech, Inc. ATTN: Technical Library 630 North Rosemead Blvd. Pasadena, CA 91107
2	TRW Systems Group ATTN: Benjamin Sussholtz Tech Info Ctr/S-1930 One Space Park Redondo Beach, CA 90278
1	TRW Systems Group ATTN: Greg Hulcher San Bernardino Operations P. O. Box 1310 San Bernardino, CA 92402
2	Union Carbide Corporation Holifield National Laboratory ATTN: Doc Control for Tech Lib Civil Defense Research Proj P. O. Box X Oak Ridge, TN 37830
1	Universal Analytics, Inc. ATTN: E. I. Field 7740 W. Manchester Blvd. Playa del Rey, Ca 90291
1	Weidlinger Assoc. Consulting Engineers ATTN: M. L. Baron 110 East 59th Street New York, NY 10022
1	Westinghouse Electric Company Marine Division ATTN: W. A. Votz Hendy Avenue Sunnyvale, CA 94008
2	Battelle Memorial Institute ATTN: Technical Library R. W. Klingesmith 505 King Avenue Columbus, OH 43201

DISTRIBUTION LIST

No. of Copies	Organization
1	California Institute of Technology ATTN: T. J. Ahrens 1201 E. California Blvd. Pasadena, CA 91109
1	COSMIC ATTN: L. C. Gadol 112 Barrow Hall University of Georgia Athena, GA 30602
2	Denver Research Institute University of Denver ATTN: Mr. J. Wisotski Technical Library P. O. Box 10127 Denver, CO 80210
2	IIT Research Institute ATTN: Milton R. Johnson Technical Library 10 West 35th Street Chicago, IL 60616
3	Lovelace Foundation for Medical Education ATTN: Asst. Dir. of Research/ Robert K. Jones Technical Library Dr. D. Richmond 5200 Gibson Blvd, SE Albuquerque, NM 87108
1	Massachusetts Institute of Technology Aeroelastic and Structures Research Laboratory ATTN: Dr. E. A. Witmer Cambridge, MA 02139
2	Southwest Research Institute ATTN: Dr. W. E. Baker A. B. Wenzel 8500 Culebra Road San Antonio, TX 78206
2	Stanford Research Institute ATTN: Dr. G. R. Abrahamson Carl Peterson 333 Ravenswood Avenue Menlo Park, CA 94025
1	University of Illinois Consulting Engineering Services ATTN: Nathan M. Newmark 1211 Civil Engineering Building Urbana, IL 61801
2	The University of New Mexico The Eric H. Wang Civil Engineering Research Facility ATTN: Larry Bickle Neal Baum University Station Box 188 Albuquerque, NM 87131
2	Washington State University Administration Office ATTN: Arthur Miles Hohorf George Duval Pullman, WA 99163
	Aberdeen Proving Ground
	Marine Corps Ln Ofc Dir, USAMSAA ATTN: Dr. J. Sperrazza Mr. R. Norman, GWD